TECNOLOGIA SETÚBAL
ESCOLA SUPERIOR · POLITÉCNICO SETÚBAL

SAÚDE
ESCOLA SUPERIOR · POLITÉCNICO SETÚBAL

Marta da Silva Ferreira

Development of a customized 3D membrane with therapeutic adjusted to the different stages of periodontal disease

Thesis to obtain the Master of Science Degree in Biomedical Engineering

SUPERVISORS

Professor Doctor Catarina Ferreira dos Santos

Professor Doctor Joana Marques Marto

December 2023

Marta da Silva Ferreira

Development of a customized 3D membrane with therapeutic adjusted to the different stages of periodontal disease

Examination Committee

Chairperson: Prof. Dr. Célio Gabriel Figueiredo Pina, Instituto Politécnico de Setúbal
Supervisor: Prof. Dr. Catarina Ferreira dos Santos, Instituto Politécnico de Setúbal
Member of the Committee: Prof. Dr. Maria João Pedroso Carmezim, Instituto Politécnico de Setúbal

December 2023

À minha avó,
Que muito ansiou, mas não conseguiu ver o final desta etapa, mas sei que está a ver-me, seja de onde for.

Agradecimentos

Primeiramente, não poderia começar sem expressar o meu eterno agradecimento às minhas orientadoras, por toda a paciência, disponibilidade e conhecimento transmitido ao longo destes meses. À Professora Catarina Santos, por todos os conselhos, seja a nível pessoal como académico. Por não ser apenas uma orientadora e por ter estado sempre disponível para mim. Por me encorajar a sair da zona de conforto, a ter uma atitude mais positiva e especialmente, por toda a confiança depositada em mim. À Professora Joana Marto, por toda a disponibilidade, pela transmissão de confiança e conhecimento cruciais para atingir os meus objetivos. Por me dar força e me incentivar a querer saber mais e acreditar nas minhas capacidades, mesmo à distância.

Quero agradecer à Escola Superior de Tecnologia do Instituto Politécnico de Setúbal, por me fornecer os recursos, acessos e ferramentas para a realização deste trabalho.

À Faculdade de Farmácia da Universidade de Lisboa, em especial ao grupo do Dermolab, por me receberem tão bem e por me fornecerem equipamentos e materiais para a realização deste trabalho.

À Angélica Graça, pela disponibilidade infinita. Pela partilha de conhecimento e por me orientar sempre na procura de respostas. Por me motivar e me ajudar, sem nunca faltar uma palavra amiga.

À Beatriz, a minha companheira de tudo desde o início. Mesmo sendo um desafio individual para ambas, não seria o mesmo sem o apoio e presença dela. Aos meus colegas e amigos de laboratório: Daniel, Ângela, Adriana, Miguel e Bruno. Foram e são imprescindíveis para o sucesso e conclusão desta dissertação. Obrigada pelo apoio, companheirismo e pela interajuda.

Aos meus amigos, pelo suporte emocional e pela força sempre. Ao Hugo, por toda a motivação, carinho e apoio que me transmitiu ao longo destes 5 anos.

Aos meus pais e irmão, um obrigada não chega. Obrigada por me proporcionarem estar aqui, por me incentivarem sempre a querer ser mais e nunca duvidarem de mim.

Resumo

As doenças periodontais constituem um desafio significativo para a saúde, caracterizadas por inflamação crónica e deterioração progressiva do periodonto. Embora os tratamentos atuais se concentrem na remoção da placa bacteriana e na administração convencional de fármacos, persistem limitações, como danos a células saudáveis. A cirurgia periodontal é uma alternativa em casos graves, contudo, as membranas existentes não atendem adequadamente às necessidades clínicas. Com isto, surge a motivação para apresentar uma solução inovadora que emprega a tecnologia de impressão 3D para a criação de membranas gelatinosas personalizadas, incorporando propriedades específicas benéficas.

O objetivo fundamental deste estudo consistiu em formular um hidrogel multifuncional, integrando nanopartículas de Hidroxiapatite e Óxido de Grafeno, visando o tratamento de doenças periodontais. Este hidrogel foi utilizado na técnica de impressão 3D com o intuito de desenvolver uma membrana personalizada à base de gelatina, dotada de propriedades antimicrobianas, anti-inflamatórias e osteoindutoras.

Os hidrogéis multifuncionais desenvolvidos demonstraram uma reologia adequada para impressão 3D com 7,5% de GO e 2% de HAp na sua constituição. A estabilidade do hidrogel não foi afetada pela adição de componentes. A confirmação de HAp-NPs na superfície do hidrogel foi obtida e os testes de hidratação da membrana revelaram que as capacidades de absorção de água eram dependentes da temperatura, onde os hidrogéis com GO demonstraram um desempenho superior atribuído às suas interações específicas com as moléculas de água. Além disso, os resultados dos testes de tração revelaram que a incorporação do GO proporcionou melhores propriedades mecânicas. O processo de impressão 3D foi bem sucedido, com medições de porosidade que provam a possibilidade de produzir estruturas porosas com tamanhos de poros controlados.

Estes resultados conduziram ao desenvolvimento bem-sucedido de hidrogéis multimateriais à base de gelatina. Estes hidrogéis exibiram propriedades reológicas favoráveis, estabilidade estrutural, resistência mecânica e excelente capacidade para ser impresso recorrendo à tecnologia de impressão 3D, assegurando resultados confiáveis e reprodutíveis. Essa eficácia sugere que esses hidrogéis podem ser aplicados no contexto do tratamento de doenças periodontais.

Palavras-Chave: Doenças periodontais; Impressão 3D; Membrana personalizada; Nanopartículas de Hidroxiapatite; Óxido de Grafeno

Abstract

Periodontal disease poses a significant health challenge, leading to chronic inflammation and progressive deterioration of the periodontium. Current treatments focus on plaque removal and conventional drug delivery methods, but limitations exist, such as damage to healthy cells. Periodontal surgery is an option in severe cases, but available membranes do not meet clinical needs. This motivates the proposal of an innovative solution using 3D printing technology to create personalized gelled membranes with specific beneficial properties.

The work aims to produce a multifunctional gelled hydrogel incorporating Hydroxyapatite nanoparticles and Graphene Oxide for treatment of periodontal disease. This hydrogel will be applied in 3D printing technology to create a personalized gelled membrane with antimicrobial, anti-inflammatory, and osteoinductive effects.

The multifunctional hydrogels demonstrated optimized rheology for 3D printing with 7.5% of GO and 2% of HAp. The hydrogel's stability remained unaffected by the addition of components. Confirmation of HAp-NPs on the hydrogel surface was achieved and water stability tests revealed that water absorption capacities were temperature-dependent, with GO-containing hydrogels demonstrating superior performance attributed to their specific interactions with water molecules. Furthermore, the results of the tensile tests reveal that the incorporation of GO has led to improved mechanical properties. The 3D printing process was successful, with porosity measurements that demonstrate the possibility of producing porous structures with controlled pore sizes.

These results proved the successful development of gelatin-based multimaterial hydrogels. These hydrogels demonstrated favorable rheological properties, structural stability, mechanical strength, and excellent 3D printing capabilities, guaranteeing reliable and reproducible results, suggesting that they can be applied in the treatment of periodontal diseases.

Keywords: Periodontal disease; 3D printing; Personalized membrane; Hydroxyapatite nanoparticles; Graphene Oxide

Table of Contents

Agradecimentos i

Resumo ii

Abstract iii

List of Figures viii

List of Tables xi

List of Abbreviations xii

Chapter 1 - Introduction 1

1.1. Motivation 1

1.2. Identification of the problem 1

1.3. Aims 1

1.4. Organization of the Dissertation 2

Chapter 2 - Literature Review 3

2.1. Periodontal Disease – Anatomy of the periodontium 3

2.2. Current treatment modalities for periodontal disease 6

2.3. 3D printing technology for periodontal regenerative applications 7

2.3.1. Extrusion-based printing 9

2.3.2. The role of rheological properties with printing behavior 10

2.4. Compounds added to the 3D gelatin-based hydrogel membrane 12

2.4.1. Gelatin 13

2.4.2. Tannic Acid 14

2.4.3. Betaine 16

2.4.4. Polyvinyl alcohol 17

2.4.5. Graphene Oxide 18

2.4.6. Hydroxyapatite nanoparticles 19

2.5. 3D printed membranes for periodontal regeneration 21

Chapter 3 - Materials and Methods **23**
3.1. Materials 23
3.2. Preparation of Gelatin-based hydrogels' ink 23
3.3. Production of Hydroxyapatite nanoparticles 23
3.4. Characterization of Hydroxyapatite nanoparticles 24
3.5. Incorporation of compounds in control formulation 25
3.6. Characterization of Gelatin-Based Hydrogels 25
3.6.1. Rheological characterization 25
3.6.2. ATR-FTIR Spectroscopy 26
3.6.3. Scanning Electron Microscopy 26
3.6.4. Energy Dispersive Spectroscopy 26
3.6.5. Water Stability 27
3.6.6. Degradation Ratio 27
3.6.7. Tensile Tests 28
3.7. 3D Printing 29
3.7.1. Line test 30
3.7.2. Printing parameters 30
Chapter 4 – Results and Discussion **33**
4.1. Characterization of Hydroxyapatite nanoparticles 33
4.2. Characterization of Ink Formulations 34
4.2.1. Rheology Properties 34
4.3. Characterization of Gelatin-based Hydrogels 41
4.3.1. The effect of the addition of HAp and GO to the hydrogel 41
4.3.2. Water Stability 47
4.3.3. Degradation Ratio 50
4.3.4. Mechanical Properties 52
4.4. 3D Printing Process 54

4.4.1. Strand and line tests 54
4.4.2. 3D Printed Constructs 56
4.4.2.1. Porosity measurements 56
Chapter 5 - Conclusion and Future Work 59
5.1. Conclusion 59
5.2. Future work 60
References 61

List of Figures

Figure 1 - Periodontal histopathology [5]. 4

Figure 2 - Tooth section showing periodontal ligament anatomy with typical distribution of PDL fibers in both physiological and pathological conditions [8]. 5

Figure 3 - Extrusion-based printing process. 10

Figure 4 - Flowchart of the hydrothermal process. 24

Figure 5 - Specimen geometry and measurements used in tensile tests. 28

Figure 6 - Diagram explaining the cross-sectional area of the specimen. 29

Figure 7 - Allevi 2 [73]. 30

Figure 8 – Nozzles used for printing the 3D hydrogel inks. The pink and white nozzles are metal tips with 27 Gauge and 25 Gauge, respectively. Pictures retrieved from [73]. 31

Figure 9 - Illustration of two designs produced. The three layers individually and the final three-layered patch. The first, second and third layers have an angle of 45°, 90°, 135°, respectively. All layers were printed with 0.15 mm layer height, 30 mm/s printing velocity and 0.6 mm. ... 32

Figure 10 - ATR-FTIR spectrum of hydroxyapatite nanoparticles. 33

Figure 11 - Transmission Electron Microscopy images of hydroxyapatite nanoparticles. 34

Figure 12 - Rheological temperature sweep of gelatin-based formulations – Group_GO37.5. (A) GEL30 (Control formulation). (B) GEL30-HAp0.1. (C) GEL30-GO37.5. (D) GEL30-GO37.5-HAp0.1. 35

Figure 13 - The role of viscosity in printing process. A - Analysis of viscosity with temperature. B - Strand test showing over-gelation through printing at 50ºC. 37

Figure 14 - Isothermal analysis on GEL30-GO37.5-HAp0.1. 37

Figure 15 - Rheological temperature sweep of gelatin-based formulations – Group_GO7.5. (A) GEL30 (B) GEL30-HAp2. (C) GEL30-GO7.5. (D) GEL30-GO7.5-HAp2. 39

Figure 16 - Analysis of viscosity with temperature. The three types of gelation identified in GEL30-GO7.5-HAp2. 40

Figure 17 - ATR-FTIR spectrum of Group_GO37.5 gelatin-based hydrogels. 42

Figure 18 - ATR-FTIR spectrum of Group_GO37.5 gelatin-based hydrogels. 43

Figure 19 - SEM images of Group_GO7.5 gelatin-based hydrogels. (A) GEL30, (B) GEL30-GO7.5, (C) GEL30-HAp2 and (D) GEL30-GO7.5-HAp2. 44

Figure 20 - Energy-dispersive X-ray spectroscopy mapping of GEL30-HAp2, including SEM image (A), Calcium element (B), Phosphate element (C) and EDXS spectrum of GEL30-HAp2 hydrogel (D). 45

Figure 21 - Energy-dispersive X-ray spectroscopy mapping of GEL30-GO7.5-HAp2, including SEM image (A), Carbon element (B), Calcium element (C), Phosphate element (D), Sodium element (E) and Oxygen element (F). 46

Figure 22 - EDXS spectrum of GEL30-GO7.5-HAp2 hydrogel. 47

Figure 23 - Water-absorption capacity of the gelatin-based hydrogels stored at 25ºC and 4ºC. The assay was performed at 25ºC. (A) Visual results of the GEL30-GO7.5, GEL30-GO7.5-HAp2 and GEL30-HAp2 hydrogels at the initial (T0) and final times (Tf). (B) Graph displaying the behavior of the hydrogels based on equation 2. 48

Figure 24 - Water-absorption capacity of the gelatin-based hydrogels stored at 25ºC and 4ºC. The assay was performed at 37ºC. (A) Visual results of the GEL30-GO7.5, GEL30-GO7.5-HAp2 and GEL30-HAp2 hydrogels at the initial (T0) and final times (Tf). (B) Graph displaying the behavior of the hydrogels based on equation 2. 49

Figure 25 - A film formed on the exposed surface of the hydrogel control after one day of oxygen exposure. 50

Figure 26 - Degradation ratio (%) of the gelatin-based hydrogels dried for 15 days. These hydrogels were tested for 21 days in PBS solution. (A) Visual results of the GEL30, GEL30-GO7.5, GEL30-GO7.5-HAp2 and GEL30-HAp2 hydrogels at the initial (T0) and final times (Tf), after 21 days. (B) Graph displaying the behavior of the hydrogels based on equation 3. 51

Figure 27 - Tensile testing. (A) Hydrogel specimens after their production. (B-C) The tensile test before and after fracture, respectively. (D) Stress-Distance curves are representative of all the hydrogels. 53

Figure 28 - Strand tests. Different temperatures result in different types of gelation. 54

Figure 29 - Line test. Printed filaments to obtain length and width index measurements. 55

Figure 30 - 3D printed constructs of all the formulations in two different geometries. 56

Figure 31 - GEL30-HAp2 and GEL30-GO7.5-HAp2 gum patches with 30x and 100x magnification, respectively. 57

Figure 32 - Porosity of GEL30-GO7.5-HAp2 at 400x magnification. 58

List of Tables

Table 1 - Advantages and disadvantages of basic 3D printing techniques. Adapted from [24]–[27]. 9

Table 2 - Qualitative and quantitative composition of all formulations. 25

Table 3 - Printing parameters used in all gelatin-based hydrogel formulations..... 32

Table 4 - Rheological parameters of all final formulations..... 41

Table 5 - Ca/P ratio present in GEL30-HAp2 hydrogel patches. 45

Table 6 - Ca/P ratio present in GEL30-GO7.5-HAp2 hydrogel patches. 47

Table 7 - Area average and standard deviation of the pores presented in Figure 32. 58

List of Abbreviations

2D – Two-dimensional

3D - Three-dimensional

AG – Alginate

ATR – Attenuated total reflectance

BMSCs - Bone Marrow Stromal Cells

EDS - Energy Dispersive Spectroscopy

EDXS - Energy dispersive X-ray spectroscopy

FTIR – Fourier Transform Infrared

GAA - Gum Arabic Aldehyde

GCF - Gingival Crevicular Fluid

GO – Graphene Oxide

HAp – Hydroxyapatite

HAp-NPs – Hydroxyapatite' nanoparticles

hDPSCs - Human dental pulp stem cells

HFE - Hydrogel-forming extrusion

ISO – International Organization of Standardization

L – Length

L' – Length Index

LAP - Lithium phenyl-2,4,6-trimethylbenzoylphosphinate

NPs – Nanoparticles

PBS - Phosphate Buffered Saline

PDL - Periodontal ligament

PEG – Polyethylene glycol

PGO - Polydopamine-mediated graphene oxide

pH – Potential of hydrogen

PHA - Polydopamine-mediated hydroxyapatite

PMN - Polymorphonuclear neutrophils

PVA - Polyvinyl alcohol

SA – Sodium alginate

SEM - Scanning Electron Microscopy

TA – Tannic Acid

TCPS - Tissue Culture Polystyrene

TEM - Transmission Electron Microscopy

TIPS - Thermally Induced Phase Separation

W – Width

w/v – Weight/Volume

W' – Width Index

Wf – Final Weight

Wi – Initial Weight

Wt – Specific time weight

wt% - Weight percentage

Chapter 1 - Introduction

1.1. Motivation

This dissertation is motivated by the need to improve the efficacy and individualization of periodontal disease treatment using 3D printing technology. The personalized aspect of 3D printing technology allows the production of patient-specific gelled membranes that are customized to an individual's unique anatomical and pathological features. The study aims to utilize state-of-the-art biocompatible materials and precise 3D printing techniques to enhance the regenerative capacity of the membranes. The treatment approach prioritizes patient outcomes, compliance, and aligns with current healthcare practices. The dissertation seeks to address gaps in current periodontal treatment options through the exploration of innovative solutions that integrate regenerative medicine and 3D printing technologies. Ultimately, this research aims to advance biomedical applications with a focus on personalized and regenerative approaches to managing periodontal disease.

1.2. Identification of the problem

Periodontitis is a chronic inflammatory disease of the periodontium, a structure composed of the tissues that surround and protect the teeth. This disease, in an advanced form, is characterized by the loss of the periodontal ligament and the destruction of the surrounding alveolar bone. Periodontal disease is the leading cause of tooth loss and is the most common oral condition in humans. Problems identified in the current treatment of periodontal disease are the lack of personalization, inadequate regenerative potential, inefficient conventional manufacturing processes, limited integration of technological advances, insufficient interdisciplinary collaboration, and cost-related barriers to advanced treatment. These challenges emphasize the necessity for innovative solutions, specifically in utilizing 3D printing technology for creating individualized and regenerative membranes. The dissertation seeks to resolve these challenges by proposing a novel strategy that combines advanced materials and precise 3D printing techniques to improve treatment outcomes and accessibility, while promoting interdisciplinary collaboration in healthcare [1].

1.3. Aims

The aim of this dissertation was to use 3D printing technology to create personalized and multimaterial gelled membranes with specific properties such as antimicrobial, anti-

inflammatory, and osteoinductive effects that has the potential to revolutionize the field of regenerative medicine, focusing on morphology of the lesion and clinical stage of the periodontal disease.

1.4. Organization of the Dissertation

The work is divided into 5 chapters and their respective subtitles to make reading easier and more straightforward.

This initial chapter will present the principles, aims and organization of this dissertation. Chapter 1 is fundamental for the understanding of the main elements of this work. Chapter 2 provides a comprehensive review of the literature, beginning with an exploration of periodontal disease and the anatomy of the periodontium. It then reviews the current treatment modalities for periodontal disease, leading to an examination of 3D printing technology for regenerative applications in this context. The roles and contributions of various compounds incorporated into the 3D gelatin-based hydrogel membrane are described in detail. The chapter concludes with an analysis of prior research on periodontal regeneration utilizing 3D printed membranes.

The following chapter presents the materials and methodology utilized in this study. Chapter 3 is organized into multiple sections. The materials used in the work are listed comprehensively, followed by a detailed description of the preparation and production processes for key components, such as gelatin-based hydrogels and hydroxyapatite nanoparticles. Furthermore, the chapter outlines the characterization techniques used. The section on 3D printing includes specific tests and parameters implemented during the printing process.

The Results and Discussion section is presented in Chapter 4. This chapter outlines the crucial findings of the dissertation. The analysis for hydroxyapatite nanoparticles, ink formulations, and gelatin-based hydrogels is detailed, with each aspect of the results discussed in depth, and the implications of the findings for the development of personalized membranes for periodontal regeneration are considered. The chapter concludes with insights into the 3D printing process and its implications for the overall research objectives.

The final chapter is Conclusion and Future work, offering a concise summary of the key findings, drawing conclusions based on the results and discussions presented in Chapter 4. It also explores future outlooks and potential directions for further research, providing a forward-looking view of the application of 3D printing technology in the treatment of periodontal disease. This final chapter serves as a comprehensive conclusion to the dissertation, summarizing the contributions to the field and suggesting directions for future research.

Chapter 2 - Literature Review

This chapter will overview the research conducted to support all theory and practical work undertaken in this dissertation. The literature review provides further insight into what already exists and what viable directions to pursue.

2.1. Periodontal Disease – Anatomy of the periodontium

Periodontal disease is characterized by chronic inflammation and progressive deterioration of the soft and hard tissues of the periodontium [2] - a term used to describe the supportive apparatus surrounding the tooth - leading to receding gums and loss of the bone supporting the teeth. Periodontal disease is described in two stages: gingivitis and periodontitis. Gingivitis represents the initial stage of periodontal disease, characterized by inflammation that is localized to the gingival tissues due to bacteria in dental plaque and is transient, non-progressive and typically reversible with appropriate intervention such as dental prophylaxis and consistent home care. However, it can progress to periodontitis. Periodontitis is the inflammation of the entire periodontium which extends to the jawbone and is irreversible [3]. It is the later stage of the disease process and is defined as the inflammation of the deeper supporting structures of the tooth caused by microorganisms [4].

The histopathology of periodontal diseases can be characterized in four distinct stages of disease progression and each stage considers both clinical and histopathological appearances of tissues: initial, early, established, and advanced lesions, as demonstrated in Figure 1.

The initial lesion is marked by a plaque that results in the increased amounts of gingival crevicular fluid (GCF) due to intercellular gap formation and vascular changes in response to the initial trauma, attracting polymorphonuclear neutrophils (PMN) to the site of the lesion and T lymphocytes are responsible to alter specifically the fibroblasts of the affected area. Clinically, this stage of the lesion is benign. In the second stage, known as the early lesion, the initial injury is characterized by redness. During this phase, PMNs facilitate the resolution of the lesion by clearing the fibroblasts that are undergoing apoptosis [4] and simultaneously disintegrate the collagen fibers. Consequently, this process generates a widening of the pre-existing space, thus facilitating the infiltration of immune cell constituents. The next stage, the established lesion, is dominated by leukocyte aggregation and B cells, either plasma cells or lymphocytes [4]. This process will lead to the transformation of the side of the lesion, changing the junctional and sulcular epithelium to an extremely vulnerable epithelium called the pocket

epithelium and commonly visible through bleeding after light gingival manipulation. Finally, the last stage is advanced lesion that is a transition to periodontitis. The advanced lesion is created by the migration of biofilm to the pocket, which gives an ideal niche for anaerobic bacteria to proliferate. This stage is characterized by the loss of gingival fibers and alveolar bone [3]. This disease is often the result of incorrect treatment of gingivitis, which is defined as inflammation of the gums resulting from the accumulation of bacteria between the gums and the tooth.

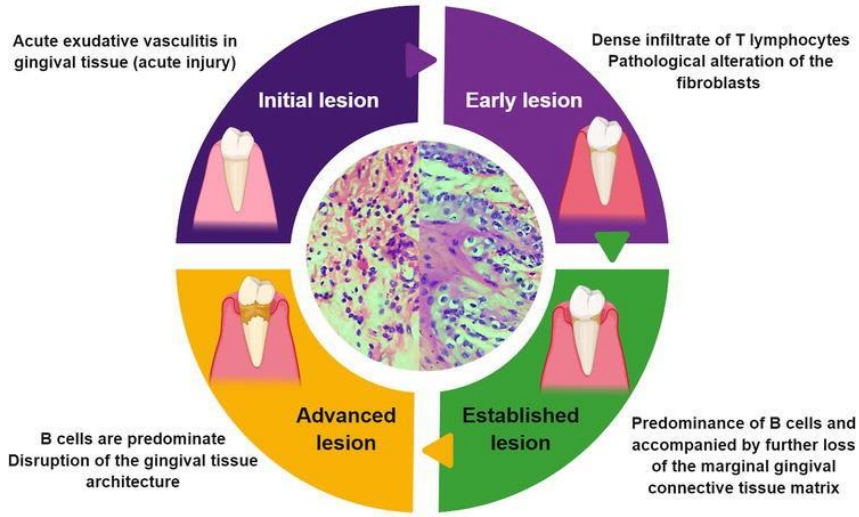

Figure 1 - Periodontal histopathology [5].

Periodontal diseases can manifest in several ways. Most early stages of periodontal diseases go unnoticed because they are asymptomatic inflammatory responses in the oral cavity. The first reported symptom of periodontal diseases is often bleeding while brushing or flossing. Another symptom that patients may notice is halitosis. Periodontitis acts silently, showing few symptoms, but can gradually develop over the years, including sensitive, red, and swollen gums; plaque on the teeth; pain when chewing; sensitive and/or wobbly teeth; new gaps between the teeth; receding gums; changes in bite and, most seriously, tooth loss [6]. Over time, and if left untreated, periodontitis can cause inflammation and damage to the gums and bones, leading to tooth loss while compromising mastication and affecting the quality of life [7].

This condition is common and can range in severity from mild gum inflammation to severe damage to the supporting structures of the teeth. In its severe form, periodontitis is the sixth most prevalent condition in the world, afflicting about 10% of the adult population.

Periodontal diseases involve periodontium, a dynamic structure made up of connective tissue that supports the teeth, enables occlusal relationships, and protects the teeth against oral microflora. Periodontium is made up of the gingiva, the mucosa and alveolar bone, cementum,

and the periodontal ligament (PDL). An illustration of the healthy tooth and periodontitis with periodontal ligament anatomy is shown in Figure 2.

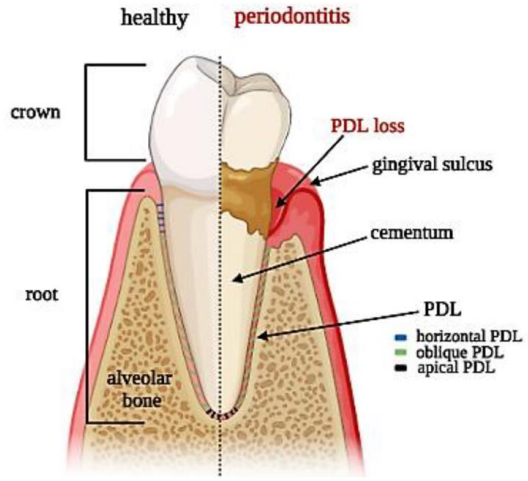

Figure 2 - Tooth section showing periodontal ligament anatomy with typical distribution of PDL fibers in both physiological and pathological conditions [8].

These components serve to support the teeth in their alveolar bone. The tissues typically seen on clinical inspection are only those of the oral mucosa. The oral mucosa can be divided into three types: the masticatory, lining, and specialized mucosa.

The gingiva is firmly bound to the underlying alveolar bone [9] and is continuous with the alveolar mucosa that is situated apically and is unbound [10]. It consists of two main parts: a free gingival margin and the attached gingival margin. The free gingiva surrounds the tooth above the gum line and is not directly attached to the tooth surface and the attached gingiva is firmly attached to the underlying bone and tooth surfaces.

The alveolar bone is the largest structural element supporting the teeth and is covered by soft connective tissues such as the attached gingiva and the alveolar mucosa [11]. Cementum is a mineralized tissue that protects the surface of tooth roots, promoting dental and periodontal attachment and is known to be the site of PDL attachment. This tissue is formed continuously throughout life because there is a continuous formation of new layers of cementum that are deposited to keep the attachment intact as the surface layer ages [12].

The PDL is responsible for providing support and anchorage to the tooth, allowing it a slight degree of movement within the alveolus, which is essential for distributing occlusal forces during mastication and avoiding excessive stress on the tooth and surrounding structures [8]. It is also part of its function to respond to inflammation and infection through immune responses to fight pathogens and restore tissue health, however, in chronic cases, inflammation can lead to tissue damage and progress to periodontal disease. On the other

hand, periodontium is capable of repairing and regenerating tissues by using regenerative therapies to promote the regeneration of tissues damaged by disease, injury, or surgical procedures. Finally, saliva plays a key role in maintaining oral health, offering lubrication to oral tissues, providing enzymes for digestion, and contributing to the remineralization of teeth. Proper oral hygiene practices are essential for preventing the build-up of dental plaque and maintaining periodontal health. Proper oral hygiene practices are essential to prevent dental plaque build-up and maintain periodontal health [13].

2.2. Current treatment modalities for periodontal disease

Periodontal diseases are treated according to their severity and, consequently, the solutions can be surgical or nonsurgical options. Currently, most of the available treatments focus on removing the bacterial plaque and tartar from the gums and teeth so that the affected tissues can heal. The nonsurgical treatments are applied when the disease is not advanced, involving less invasive procedures, including scaling, where the tartar and bacteria from the tooth and below gumline are removed; root planning; the root surfaces are smoothed, preventing further buildup of tartar and bacteria and the re-attachment of the teeth to the gums and antibiotics, topical and oral antibiotics can help control bacterial infection [1]. In more severe cases, periodontal surgery is performed to clean deep pockets between the teeth and gums, repositioning the gum tissue around the teeth [14].

Some surgical procedures are performed to provide a more in-depth treatment. Flap surgery exposes the tooth roots for more effective scaling, root planning and, due to periodontitis often causing bone loss, the underlying bone may be reshaped before the gum tissue is stitched back in place. Other options include soft tissue grafts, by removing a small amount of tissue from the roof of the mouth or using tissue from another donor source and attaching it to the affected site, this is usually done because this disease causes loss of gum tissue and the gumline gets lower, exposing some of tooth roots. Bone grafting is an option when periodontitis destroys the bone around the tooth root, the graft may be made from small bits of the patients own bone or artificial material or donated. This technique helps prevent tooth loss by holding the tooth in place and serves as a platform for regrowth of natural bone. To stimulate the regrowth of the bone, guided tissue regeneration and tissue-stimulating proteins are performed. The guided tissue regeneration by placing a special type of fabric between existing bone and tooth, preventing the unwanted tissue from growing into the healing era. Tissue-stimulating proteins involves the application of a gel containing the same proteins found in

developing tooth enamel to a disease tooth root and stimulates the growth of healthy bone and tissue [13, 15].

The conventional solutions that already exist have several challenges because it results in poor biodistribution, poor selectivity and release of the therapeutic effect, and damage to healthy cells [16]. Since the membranes marketed do not fit the real clinical needs, this work proposes the development of a 3D gelled membrane personalized with antimicrobial, anti-inflammatory and osteoinductive effect, through 3D printing, adjusted to the morphology of the lesion and clinical stage of the disease. Regardless of all the challenges they face, nanotechnology has made many advances in the field of biomimicry and has shown great potential in the regeneration of hard and soft dental tissues. To enhance the effectiveness of scaffold therapy, regenerative biomaterials in the form of nanosized materials have been recently used. These biomaterials exhibit nanostructured surfaces, which increase the surface area to achieve high roughness and wettability [17]. With the addition of numerous nanomaterials, many clinical benefits have been produced in dental medicine using tissue engineering properties, such as advanced treatments for caries and periodontal disease, bone regeneration, viable biological repair of teeth after caries and, in the near future, perhaps achieving the complete regeneration of lost teeth [18].

2.3. 3D printing technology for periodontal regenerative applications

Currently, treatment options for replacing damaged organs and tissues depend on obtaining tissue from the patient themselves or through transplants, making them limited treatments, both due to the scarcity of donors and the lack of more effective substitutes. 3D printing has emerged with the need to break this barrier and create tissue and organ alternatives for artificial transplants. This type of printing allows producing desired sizes and shapes, as well as various types of scaffolds with greater precision [18]. Recently, with the need to progress, 3D printing technology converged with biological and material sciences, creating a new tissue engineering technique called 3D bioprinting. This technology has been extensively studied with the aim of increasing the functionality of tissue engineering constructs through the development of implants seeded with cells that support native tissues in terms of anatomical geometry, cell placement and their microenvironment. With these artificial structures, it will be possible to promote the necessary mechanical support, sufficient transport of nutrients suitable for integration into the systemic circulation and the incorporation of multiple cell types for tissue regeneration [19]. Since this method of printing employs live cellular material, it requires a controlled environment, biological expertise, and specific sterilization conditions, which is why 3D printing is more reproducible and can more easily print different types of materials.

3D printing is an additive manufacturing process that deposits biomaterials, cells, and other bioactive molecules, layer by layer, to fabricate complex structures with micrometric precision similar to 3D tissue. This type of printing makes it possible to customize multi-material implants to patient-specific geometries for medical prostheses. The biggest challenge facing 3D printing is the selection of the formulation materials for this application, i.e. the ink [19]. For this process to occur, the deposited materials are printed through inks - a solution of one biomaterial or a mixture of several biomaterials in hydrogel form - that play the role of printing substrate and as a scaffold. These biological constructs aim to reproduce the architectural, physiological, and mechanical properties of native tissue. Furthermore, when compared to other methods of structure preparation, such as thermally induced phase separation (TIPS) and electrospinning, the use of 3D printing allows for a more flexible, customized, and repeatable structure. Due to the excellent properties of hydrogel, such as high biocompatibility and processability [20].

In the last years, the development and applications of this method have increased considerably due to its advantages: control and precision; and a wide variety of materials to produce personalized membranes. In addition, this printing can be used to control the porosity of scaffolds and introduce interconnected channels [21]. During the printing process, inks can be cross-linked or stabilized during or immediately after printing to give their final desired shape and structure. Inks can be produced using natural or synthetic biomaterials individually, or a combination of both as hybrid materials and, to be considered as ideal as possible, must have adequate mechanical, rheological, and biological properties for the target tissues, which are essential to ensure the correct functionality of the printed tissues and organs [22].

The three main printing techniques are: inkjet, laser-assisted, and extrusion printing (Table 1). Inkjet printing was the first technology created and is very similar to conventional 2D inkjet printing, in which the ink is stored at an ink cartridge connected to a printhead and, during the process, acts as the source of ink, controlled electronically. Laser-assisted printing originated from direct laser engraving and laser-induced transfer technologies, this works with a donor layer - a "ribbon" structure with an energy-absorbing layer at the top and an ink solution layer at the bottom - that responds to laser stimulation. During printing, a focused laser pulse is applied to stimulate a small area of the absorbing layer. This laser pulse vaporizes a portion of the donor layer, giving rise to a high-pressure bubble at the interface of the bottom layer, propelling the suspended ink. After the impulse, the droplet of solution is stored on the receiving substrate and consequently cross-linked. Finally, the extrusion printing technique is a modification of inkjet printing, with the particularity that it can print viscous materials and uses an air force pump or a mechanical screw plunger to dispense inks. In this work, the 3D printing

technique used was extrusion, due to it being the most efficient when applied to a hydrogel [23].

Table 1 - Advantages and disadvantages of basic 3D printing techniques. Adapted from [24]–[27].

3D Printing Techniques	Advantages	Disadvantages
Extrusion-based	Wide range of materials	Viscosity and temperature of materials
	Good mechanical properties	Low printing speed
Laser-based	Wide range of materials	Heat effects
	Accurate and fast printing	Long fabrication time
Inkjet-based	High gelation speed	Low mechanical and structural integrity
	High efficiency	Limited choice of materials

2.3.1. Extrusion-based printing

Extrusion is the most common printing technique (Figure 3) due to its exciting developments in fabricating organized tissue constructs by dispensing, at the same time, cells, and matrix materials to repair and replace damaged tissues. In this technique, the biomaterials are loaded into cartridges and extruded using pneumatic pressure or mechanical forces through a nozzle onto a pre-defined point on a fabrication platform. The cartridges are positioned onto an XYZ stage, with temperature and pressure being set by the user through the software by the computer [22]. If applied with a continuous force, rather than a single drop of ink, this type of printing can print continuous cylindrical lines and can be able to print a wide list of materials [20]. The advantages of this printing technique are its ability to extrude inks with different compositions and rheological properties. The rheological studies of inks are essential to find the best extrusions conditions for printing, including viscosity, gelation and melting temperature; the extrusion printing enables the operator to create heterogeneous models by depositing different types of inks at predefined locations within a pre-engineered structure, improving the control of biological function by promoting the organization and cellular heterogeneity of the tissue. Finally, one of the most important advantages, the extrusion-based printing has become relatively affordable, and the instrumentation can be highly customizable with respect to the desired structure or ink. Currently, extrusion printers can be customized for specific applications that enable core-shell printing, combined extrusion, electrospinning, and UV curing during and post-printing in addition to other emerging tissue engineering technologies.

This technology allows the 3D Hydrogel-forming extrusion (HFE), a printing process that describes the computer-controlled layer-by-layer dispensing of semi-solid polymeric solutions, dispersions or pastes through a movable nozzle in (x,y,z) coordinates, to create a 3D structure. The term "hydrogel-forming" refers to the use of polymers that react through physical, ionic, or radiation crosslinking to enable the gelation of the 3D printed construct. These hydrogels are produced from a wide range of polymers of natural origin, such as gelatin, alginate, and chitosan, and of synthetic origin, such as polyethylene glycol (PEG) or polyvinyl alcohol (PVA). Materials with distinctive characteristics are frequently incorporated to enhance the performance of hydrogels and, as a result, improve their physicochemical properties. Additionally, these materials can enhance the overall functionality and applicability of 3D structures. The selection of polymers depends on objective factors like biocompatibility, production cost and method, rheological and mechanical attributes, extrusion mechanism, applicability, and the intended function of the 3D structure [28].

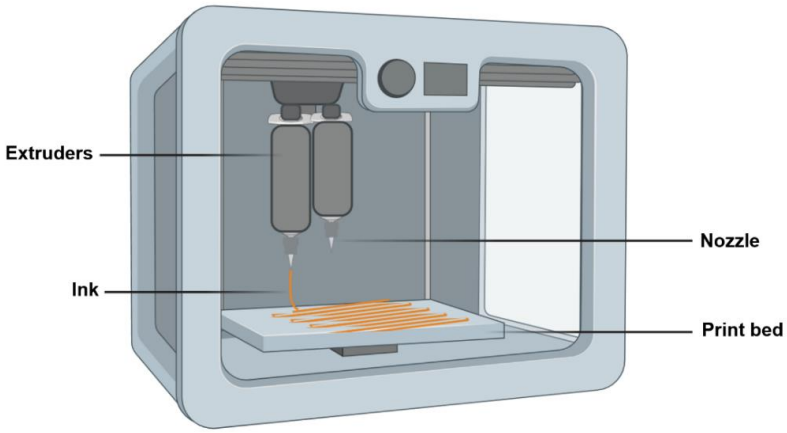

Figure 3 - Extrusion-based printing process.

2.3.2. The role of rheological properties with printing behavior

3D printing continues to be a challenge in finding materials with optimal properties and the rheological behavior required for print stability. Fluid rheology is essential in evaluating printability, particularly for its applicability as a hydrogel in 3D printing via semi-solid extrusion. Shape accuracy and reproducibility of the printing process are substantially influenced by the fluid's behavior [29].

Rheology is the study of the flow behavior of materials under the application of an external force or deformation [30]. This study is crucial to understanding the behavior and viscosity of the fluid to assess its printability.

The rheological behavior of the hydrogel in formation is monitored as a function of temperature, following the shear storage modulus G', which characterizes the elastic behavior, and the loss modulus G'', which is responsible for characterizing the viscous part of the viscoelastic behavior. The values of G′ correspond to the stored energy, reflecting the elastic behavior of a material when deformed; while G″ represents the deformation energy that is lost due to internal friction during the shearing process, reflecting the flow of a material [29].

The rheological properties of a hydrogel are the basis for determining its printing parameters and printability. Rheology is the study of flow and deformation of a matter under the condition of an external force, which is highly relevant to an extrusion-based 3D bioprinting process. Bom *et al.* [31] studied the correlation between rheological properties with printing behavior. The 3D printing process optimization should be initiated with rheology studies, in order to evaluate ink's behavior. The ink begins in a resting state inside the cartridge with no initial flow. However, when applied forces act on it, it then undergoes deformation and starts to flow in high shear conditions as it passes through the nozzle walls. Thereafter, it takes on a new shape until it ultimately returns to a new resting state. The rheological properties that are critical to these transitions include viscosity, viscoelastic shear modulus, viscosity recovery behavior, and shear stress, all of which are linked to the ink's performance prior to (rest and flow initiation), during (extrudability flow behavior), and after printing (shape fidelity, printing accuracy, and adhesiveness) [31].

Viscosity is the resistance of a fluid to flow during the application of stresses and influences extrudability, printing accuracy and shape fidelity. Low viscosity hydrogel inks can minimize nozzle clogging during printing but often result in poor printing accuracy. Hydrogels inks with higher viscosity usually retain shape after extrusion, however, an increase in viscosity requires an increase in the extrusion shear stress. To avoid the extrusion shear stress, the extrudability can be controlled by adjusting printing parameters or using different nozzle geometries or sizes [31].

Rheological behavior of Gelatin

The development of gelling systems is an area of particular interest in gelatin rheology. The sol-gel transition involves a crosslinking polymer that undergoes a phase transition from liquid to solid state at a critical point, known as the "gel point." Crucial properties for gelatin gels are gel strength and gel melting point which depend on factors such as concentration, molecular weight, the formation of complexes by the amino acid composition, and the ratio of α/β chains present in the gelatin. Moreover, the content of α-chains within gelatin determines its gel

strength. As a result, gelatin with a higher number of α-chains exhibits stronger gelling properties [32].

Viscosity is a significant factor for evaluating gel strength in gelatin. It is influenced by factors such as molecular weight, pH and concentration. Commercial gelatins currently have viscosities ranging from 2.0 to 7.0 mPa-s, with some even reaching 13.0 mPa-s. The lowest viscosity was observed in the higher pH range of 6-8, while the highest viscosity was observed in the lower pH range [32].

When applying gelatin to 3D printing, it is important to understand that would require adequate control over the physical properties of the gelatin inks. The melting point of gelatin is between 30 and 37°C, depending on their pH and concentration. Gelatin is unable to maintain its structure and would melt at physiological temperatures, so other materials are combined to improve its properties [32]. To enhance the mechanical properties of gelatin, it is vital to combine materials that are advantageous for this objective.

2.4. Compounds added to the 3D gelatin-based hydrogel membrane

The hydrogel, a porous and hydrated molecular structure, is part of a group of biocompatible polymeric materials. Its hydrophilic structure allows it to store considerable amounts of water in its three-dimensional (3D) network and can be modified to respond to external stimuli - such as light, temperature and biological signals [33]. These hydrogels are a class of 3D networks and are formed by crosslinking polymer chains dispersed in an aqueous environment, through a group of mechanisms encompassing ionic interactions and chemical crosslinking. The physical methods of gelation depend on the intrinsic properties of the polymers; however, it is an easy and reversible process without the need to modify the polymer chains. Most natural polymers can form thermally activated hydrogels, where the gelling of the hydrogel changes due to temperature variations [34]. A variety of naturally derived and synthetic polymers can be processed into hydrogels, from those formed through physical entanglement to ones stabilized via covalent cross-linking [34].

Hydrogels are widely used in 3D printing due to their ability to extrude at various temperatures depending on the components present. These polymeric structures have numerous biomedical applications, including tissue engineering.

In this work, the hydrogel is gelatin-based due to gelatin being one of the materials with the highest potential to be used as a base for hydrogels because it has hydration properties (swelling and solubility), gelling behavior, texturing, and water-binding capacity [35]. Although

it is a successful polymer in this area, it has some limitations [36]. Enhancements can be obtained by using it as a base for a hydrogel with other compounds that provide additional benefits. To combat periodontitis, gelatin has been combined with compounds with antimicrobial, antibacterial and osteoinductive properties to form a hydrogel. The materials used in this gelatin-based hydrogel are Glycerin, Tannic Acid, Betaine, Polyvinyl alcohol, Graphene Oxide and Hydroxyapatite' nanoparticles.

2.4.1. Gelatin

Gelatin is a multifunctional biopolymer with a multitude of applications across a diverse range of fields. Over several decades of research and development have led to the diverse uses of gelatin in food products, pharmacy, medicine, and cosmetics [37]. Gelatins are derived from the parent protein collagen through processes that break up the secondary and higher structures with different degrees of hydrolysis of the polypeptide backbone. The name "gelatin" comes from the Latin word "*gelata*", which describes its most important property, i.e., the formation of a gel in water [37].

Gelatin and collagen are substantially constituted by the same amino acid sequences and relative proportions, however, the physical properties of the two differ significantly. Collagen is the main constituent of all the white fibrous connective tissues present in the animal body: cartilage, tendons, the transparent sheaths that surround muscles and muscle fibers, skin and the protein matrix of bone. The major difference between these two polymers is their insolubility: while collagen is insoluble in water, gelatin is easily dissolved in water when subjected to temperatures above the denaturation temperature of native collagen [37].

Gelatin is a biodegradable and mucoadhesive polymer that have gained popularity as a vehicle in slow drug release device to deliver the antimicrobial agents. This key biomaterial has excellent properties in the formulation of tissue scaffolds and hydrogels to fulfil several applications in biomedical field [36].

The main sources of commercial gelatin are pig skin and cartilage (46%), bovine skin and bones (29.4%), and other sources (1.5%). Gelatin derived from pig is more favorable because it has a low cost, and its physical and functional properties are improved compared to other sources. In this type of source, gelatin is derived from naturally occurring collagen found in mammalian bones and skins. Gelatin produced from porcine skins is extracted using acid treatment, commonly known as Type A gelatin. In contrast, gelatin from bovine hide and bones is typically extracted using an alkaline process because they have a more complex matrix than porcine, resulting in Type B gelatin. Gelatin from mammals is the most demanded due to its

properties, with a molecular weight in the range of 10-400 kDa, allowing it to obtain distinct rheological characteristics such as high viscosity and gel strength in a variety of applications [22].

In this work, it was only used Type B gelatin. As a type of protein, gelatin obtained by the partial degradation of collagen has gained more attention as an edible film with biomedical applications due to its abundance and biodegradability. It is thermo-reversible with a melting point close to body temperature, which is particularly significant in applications for periodontal diseases due to the environment of the mouth. However, like most protein films, gelatin film does not have ideal mechanical properties due to low tensile strength and elasticity, or a water vapor barrier, which causes limitations in its application as a biomaterial. To combat this limitation, chemical and physical treatments can be applied to modify the polymer network by cross-linking the polymer chains to improve their functionality [22].

Gelatin's surface behavior such as stabilization, adhesion and cohesion, and protective colloidal function are also important reasons for its use. In addition, this polymer's biocompatibility, low toxicity, biodegradability, and antimicrobial activity make it highly suitable for a wide range of biomedical applications [35, 38].

2.4.2. Tannic Acid

Tannic Acid (TA) is a natural polyphenol, which exists in a wide variety of plants as colorless to pale yellow solid with an astringent taste. TA can be extracted from natural sources such as the bark of oak, chestnut, hemlock, and mangrove trees, but it can also be obtained from the leaves of certain sumac trees and plant branches [22]. This polyphenol is an abundant natural compound that serves as a crucial commercial raw material and has been traditionally used as a tanning agent in leather, coating, surgery, pharmaceutical and food industrial applications [22]. TA presents good antioxidative, antibacterial, hemostatic, and anti-inflammatory properties and is able to form hydrogen bonds and hydrophobic interactions with a variety of polymers [39]. It is also studied that TA could effectively enhance the mechanical strength of hydrogels [40].

Comprising water-soluble polar groups (carbonyl, phenolic functional and hydroxyl) linked to a water-insoluble hydrocarbon chain (aromatic benzene units), TA is an amphiphilic compound that can interact with organic, inorganic, hydrophilic and hydrophobic materials through hydrogen bonds, electrostatic, coordination and hydrophobic interactions. The hydroxyl groups can act as hydrogen donors or acceptors, which gives TA the ability to cross-link without chemical interaction with various molecules, polymers, and proteins. It is a weak acid and has

a wide pKa range from 2.5 to 8.5, so TA can serve as a polyanion in a medium with a pH higher than the pKa and adhere to the electrostatic interactions of other materials [41].

The chemistry of TA-based biomaterials expands from nanoparticles and thin films to bulk materials. In particular, the "gel" is a crucial category of materials in which chemical interactions have resulted in insoluble 3D molecular networks, with a large amount of solvent in their composition. TA is one of the most promising polyphenols with high molecular weight for developing new smart biomaterials for biomedical engineering [41].

Recently, the study of hydrogels with TA in their composition has seen significant development and application in the biomedical field, involving wound healing and portable sensors, using natural and synthetic polymers [41]. In the production of hydrogels, TA can be used directly in the hydrogel formulation itself or indirectly by immersing the hydrogels in a TA solution.

TA can crosslink a wide range of macromolecules through its numerous binding sites with hydrophobic coordination, electrostatic interaction, and ionic and hydrogen bonds [41]. However, TA is also capable of being a promising crosslinker in the field of synthetic and natural polymers, including alginate, chitosan, collagen and, most importantly in this study, gelatin. There are several conditions that determine the stability and performance of this type of interaction with polymers. It is crucial to analyze the concentration of TA, the pH and the type and proportion of polymers, to find a balance and optimum control of the interactions [41]. The ability of TA to be a natural phenolic cross-linker to modify gelatin and improve its mechanical performance is one of the most important characteristics in the development of this study.

TA has antibacterial, antiviral, anticancer, antioxidant and anti-inflammatory properties, giving it excellent potential for use in periodontal diseases. In addition, this polyphenol has preventive properties against a vast number of diseases that start and develop through oxidative stress, such as infections, inflammation, cancer, diabetes, and cardiovascular diseases [41].

A hydrogel composite formulation requires multiple components to achieve the desired application. Each component possesses unique characteristics, which in conjunction, will enhance the ultimate properties of the matrix. It is imperative that the materials establish strong bonds and undergo favorable reactions. The hydrogel proposed in this work has shape-memory properties.

Shape memory hydrogels can be obtained by combining TA with PVA. The key structural aspect of this hydrogel type is maintaining stronger cross-links to preserve the permanent shape and weaker ones to fix the temporary shape. TA can potentially form multiple strong H-

bonds with PVA. The stronger hydrogen bonds between PVA and TA can function as "permanent" cross-links, while the weaker hydrogen bonds between the PVA chains act as "temporary" cross-links. This allows for the creation of shape memory hydrogels [8].

When it comes to its bond with gelatin, TA is a hydrolysable tannin with multiple phenolic functionalities due to its high molecular weight. Studies explain that the amino functional groups of amino acid units in gelatin (such as lysine, arginine, and histidine) would react with phenolic reactive sites of TA under alkaline conditions to form covalent C-N bonds and generate cross-linked networks. Other reactive groups in gelatin, such as the hydroxyl group in serine units, may contribute to these reactions using a similar mechanism. In contrast, the phenolic hydroxyl and carboxyl groups of TA might bond with gelatin chains through hydrogen bonding. The degree of these reactions and interactions in gelatin/TA systems is crucial in determining subsequent material properties [42].

2.4.3. Betaine

Betaine, also known as trimethylglycine, is a short-chain, neutral, amino acid derivative [43]. It is a stable and nontoxic natural component. Betaine has some important roles such as (i) an osmolyte and (ii) a methyl-group donor. It helps to maintain the intracellular osmotic pressure due to possessing N^+ and COO^- in its molecular structure. By exhibiting minimal or no binding to protein surfaces, betaine enables cells to regulate the surface tension of water, thus stabilizing protein structure and function. Betaine is the most efficient osmolyte analyzed for albumin hydration, creating a nearly complete layer of water around the protein. It also sustains hemoglobin solvation [43].

An important characteristic of this component is its anti-inflammatory effect on diseases. Inflammation is an immune reaction and is a crucial process for host defense and wound healing. On the other hand, if inflammation is prolonged it can become the pathogenesis of various diseases and it is therefore important to use natural compounds in the treatment of diseases in order to control the intensity of the reaction. This compound is also responsible for regulating energy metabolism to relieve chronic inflammation. Disorders of this type of metabolism can lead to various chronic diseases, such as diabetes and obesity, which generally present low-grade systemic inflammation. It is therefore essential to restore normal metabolism in order to mitigate inflammation [44].

Betaine is a naturally occurring compound that has shown potential therapeutic benefits in the context of periodontal diseases.

A trial on the clinical effects of a toothpaste containing extra virgin olive oil, xylitol, and betaine in gingivitis by Rodríguez-Agurto and his colleagues [45], showed that this new toothpaste obtained the best outcomes in patients with gingivitis, showing reductions in gingival bleeding and supragingival bioflm and an increase in pH at 4 months in comparison to a commercial toothpaste. Animal studies proved that betaine suppressed the activity of NF-κB and a wide range of inflammation-related genes [44].

Another study with betaine, to evaluate its effect on immortalized human dental pulp stem cells (ihDPs) osteogenic differentiation [45], showed that ihDPs had superior proliferation ability and a longer life span and betaine promoted odonto/osteogenic differentiation via intracellular calcium regulation.

2.4.4. Polyvinyl alcohol

Polyvinyl alcohol (PVA) is a synthetic polymer used in a wide range of industrial, commercial, food and medical applications. The physical characteristics of PVA depend on how it is produced from the hydrolysis, or partial hydrolysis, of polyvinyl acetate. PVA is commonly divided into two groups, partially hydrolyzed and fully hydrolyzed. Diversifying the extent of the vinyl acetate polymer chain and manipulating the degree of hydrolysis within the contexts of alkaline or acidic environments engenders a spectrum of PVA products, exhibiting a molecular weight range spanning from 20,000 to 400,000 g/mol. This differential molecular architecture imparts discrete attributes encompassing solubility, flexibility, tensile strength, and adhesiveness to the ensuing PVA variants. Properties such as pH, viscosity, melting point, refractive index, heavy metals, are measured to characterize PVA. It is relevant to outline that these characteristic properties manifest an intrinsic correlation with both the molecular weight and the percentage of hydrolysis intrinsic to the specific grade of PVA under investigation [46].

PVA is the most used biodegradable synthetic polymer because it is a non-toxic polymer with a high capability of water absorption, chemical resistance, biodegradability, and biocompatibility properties. These properties make it a suitable polymer for the manufacture of flexible membranes for controlled drug delivery systems, including films or formulations for local application in the periodontal pocket [44].

Prakash *et al.* [47] developed hydroxyapatite nanoparticles incorporated Polyvinyl alcohol-sodium alginate (PVA-SA) films for controlled antibiotic release of amoxicillin for treating intrabody periodontal defects. PVA is known for its crystallizing nature and is a linear polymer, often combined with sodium alginate to form salt gels. The films presented high antibacterial activity against the Gram-positive and Gram-negative bacteria; highly

biocompatible and hemocompatibility. The results proved that these films can be used for periodontal defects [47].

2.4.5. Graphene Oxide

Graphene and Graphene Oxide (GO) are materials that have been studied extensively over the years, with many promising properties for a huge variety of applications.

GO is a layered carbon structure with oxygen-containing functional groups (=O, -OH, -O-, -COOH) attached to both sides of the layer as well as the edges of the plane. As with any two-dimensional (2D) carbon material, GO can also have either a single layer or multilayer structure. GO synthesis entails the oxidation of graphite, subsequently leading to the exfoliation of the resulting graphite oxide into distinct GO structures. Moreover, GO still can maintain the thinnest atomic structure compared to graphene, thus extending more active sites for functionalization [48]. The properties of the nanomaterial are intrinsically interlinked with the synthesis method, exerting a profound impact on the ensuing quantity and nature of oxygen-containing functional groups that are integrated within the GO framework.

In contrast to the hydrophobic nature of graphene, GO is hydrophilic, and it is hence relatively simple to prepare a water- or organic solvent-based suspensions. This material is a promising carrier for biomolecules and drugs. It can enhance biomaterials' bioactivity, sustainability, and mechanical performance [18]. At the nanoscale, it is presented in nanosheet form and is considered a nanomaterial that improves the mechanical and functional properties of matrices. It has good antibacterial properties [49], but in excess it can lead to toxicity.

GO plays an important role in regenerative medicine and tissue engineering, allowing the creation of a cellular niche for stem cells on the surface of a nanoparticle [50].

In the management of periodontal diseases, GO has different roles such as inhibition periodontal pathogenic biofilms, periodontal tissue regeneration and increases bone regeneration. In several studies, these materials have proven to be antimicrobial and possess remineralization properties for the management of dental caries and periodontal disease [51].

Rahmani and his colleagues [52] developed an pH-sensitive and self-healable nanocomposite hydrogel based on Gum Arabic Aldehyde (GAA)/Gelatin, graphene oxide and PVA. The PVA/GAA based hydrogel is non-toxic, water-soluble, biodegradable and pH sensitive, however, it has limitations such as poor stiffness, low mechanical strength, and hydrophilicity. GO, gelatin and boric acid were used to improve these limitations through cross-linking due to Schiff-base reaction between aldehyde groups of GAA and amino groups of gelatin, and hydrogen bonding between PVA chains and boric acid. Incorporating GO in the hydrogel

network enhanced the mechanical properties, self-healing properties, drug entrapment efficiency, and ensured the controlled release of the entrapped drug [28].

2.4.6. Hydroxyapatite nanoparticles

Hydroxyapatite (HAp), chemically known as $Ca_{10}(PO_4)_6(OH)_2$, is a biocompatible, osteoconductive, and bioactive ceramic [53]. It is the most stable calcium phosphate (CaP) biomaterial in the biological environment [54] under physiological conditions and it is considered an appropriate carrier for the controlled release of compounds. As this material shares a strong chemical resemblance with the calcium phosphate phase of human bone and teeth, is bioactive and exhibits excellent biocompatibility with various kinds of cells and tissues, synthetic hydroxyapatite has been applied and recognized as a key bone replacement material in orthopedics and dentistry. Therefore, diverse properties and varying solubility in the biological environment could potentially enhance bone formation or inhibit the proliferation of cells and tissues [54].

HAp sintered ceramics have been applied in medical and dental fields, and the applications include alveolar ridge reconstruction and augmentation and filling of bone defects [55]. In addition, due to its low solubility at physiological pH, it is used as a carrier for the local administration of drugs through surgical placement and injection [53].

HAp was primarily proposed for tissue engineering applications on hard tissues because it has excellent physico-chemical, biological, and mechanical properties [54]; however, depending on physicochemical properties, such as particle size, crystallinity degree, surface area, morphology, and surface charge, the biological response of HAp is altered [54].

Nanotechnology introduced the concept of nanostructured bioceramics, for which HAp nanoparticles have shown excellent biocompatibility and biodegradability. The surface of the nanoparticles can be modified to enable hydrophobic interactions, pi-electron density, and charge density. Furthermore, the design of the nanoparticle strongly influences the interactions with the biological environment due to their large surface-to-volume ratio, making the nanoscale material offering superior performance compared to conventional materials [55].

HAp nanoparticles and HAp nanoparticles combined with polymers have been applied to drug delivery, and the association of their physicochemical properties with biological applications has become an interesting area of ongoing research [53]. However, for their combination to be effective, it is important to find viable correlations in their properties and the reactivity/biocompatibility of the nanoparticle surface, knowing the biorelevant parameters that

will determine them, such as shape, size, functional group, morphology and crystalline phase [53].

The variety of synthesis methods enables several different nanoscale particles with different structures and morphologies to be obtained. The synthesis of hydroxyapatite' nanoparticles (HAP-NPs) can be performed by using a wide variety of methods, such as wet chemical precipitation, sol-gel processing, co-precipitation, emulsion technique, hydrothermal process, mechanochemical method, ultrasonic technique, template method, microwave processing, emulsion hydrothermal combination, and microwave hydrothermal combination [55].

Hydrothermal synthesis is a conventional method for producing low-cost hydroxyapatite NPs with a high degree of crystallinity [55]. However, when using this method, an additive is often used as a morphology shaping agent to control the morphology of the precipitated particles. In this study, the additive used to define the shape and size of the nanoparticle is citric acid. This additive, which acts not only as a reducing agent but also as a stabilizing agent [56], is used because of the chelating properties of citrate ion, as well as because of its physiological function in the Krebs cycle, producing energy in the mitochondria. Citrate also has a biological function in stabilizing the morphology of NPs in bone tissue and establishes an interface between hydroxyapatite NPs and collagen.

Citric acid as an additive has an important role in HAp synthesis, not only due to adjusting and controlling the size and morphology of precipitated products but also to stabilizing HAp. The presence of citrate is also affected by temperature: at low temperatures, the strong interation between carboxylate (-COO-) and Ca^{2+} may be attributed to the linking capacity of calcium sites that belong to two distinct primary particles of hydroxyapatite, which tend to aggregate and form larger precipitates and at higher temperatures, the interactions between citrate and calcium ions are weakened, increasing the negative surface charge in HAp nanoparticles and enabling primary particles of large aggregates to get separated from one another [39, 57].

As HAp is biomimicry material of bone and not only acts as a drug loading matrix but also to help in regeneration of deteriorated bone segments due to periodontal defects [47]. Recently, to accelerate periodontal bone regeneration in diabetes, Li *et al.* [58] produced an polydopamine-mediated graphene oxide (PGO) and nanohydroxyapatite (PHA)-incorporated conductive alginate/gelatin scaffold to modulate the diabetic inflammatory microenvironment. PHA promotes osteoinductivity and PGO provides a conductive pathway for the scaffold. This scaffold was able to promote bone regeneration by transferring endogenous electrical signals to cells and activating Ca^{2+} channels. The results also showed that this PGO-PHA-AG scaffold

had anti-inflammatory activities and induced excellent periodontal bone regeneration in diabetes [58].

2.5. 3D printed membranes for periodontal regeneration

Even though periodontitis can be treated and controlled by managing the accumulation of bacterial plaque and the resulting inflammatory response, the regeneration of lost periodontal tissues remains a major challenge in periodontology. Currently, various alternatives using 3D printing are available to manage periodontal disease or its consequences.

In recent years, several types of 3D printed hydrogels have been developed and investigated. Hydrogel-based bioinks with versatile structures and compositions that mimic the extracellular matrix of human tissues can be 3D printed to produce membranes suitable for tissue engineering applications. Mechanical properties of such membranes can be enhanced by blending them with other polymers [59]. It is possible to find in literature information justifying the application of each of the components chosen for the hydrogel developed in this work.

Raveendran *et al.* [60] studied effects of 3D bioprinting of Alginate/Gelatin hydrogel on proliferation and differentiation of human dental pulp stem cells (hDPSCs). The results showed that the 3D printed structure was more suitable for the growth of hDPSCs compared to the membranes not printed.

Vahdatinia *et al.* [59] performed an *in vivo* examination using a periodontal canine model to investigate the capability of a 3D-printed soft membrane for guided tissue regeneration. The membrane was composed of gelatin, elastin, and sodium hyaluronate, in order to be a suitable replacement for collagen. The results demonstrated higher levels of new bone formation and, after 8 weeks, the formation of periodontal tissues, bone, periodontal ligaments, and cementum was observed. In the control group, without any membranes, only connective tissue was found in the defect sites.

Graphene oxide is a widely used material to enhance the mechanical properties of hydrogels. Zhu *et al.* [61] developed a 3D printed gellan gum/graphene oxide scaffold for tumor therapy and bone reconstruction. By adding just 1.2 wt% GO, the mechanical properties of the system were improved, and the results showed that the scaffolds could support the attachment and proliferation of osteoblasts.

Since tissue-engineered bone material is an effective method to repair bone defects, Wen Qin and his collaborators [49] used 3D printing to produce GO, attapulgite and collagen composite scaffolds for bone regeneration. They achieved scaffolds with controlled pore diameter of 300–

400 µm and mechanical strength at 1.7–7.1 MPa. The results demonstrated that the addition of GO had a significant effect on the degradation of materials by retarding it. Furthermore, this 3D printed composite also promoted excellent cytocompatibility for enhanced mouse Bone Marrow Stromal Cells (BMSCs) adhesion, proliferation, and osteogenic differentiation.

Kawamoto *et al.* studied [52] the characterization and evaluation of graphene oxide scaffold for periodontal wound healing of class II furcation defects in dogs. The scaffold was prepared by coating the surface of a 3D collagen sponge scaffold with GO dispersion and was implanted into dogs to investigate the periodontal healing at 4 weeks post-surgery. The results showed that the GO scaffold exhibited low cytotoxicity, enhanced cellular ingrowth behavior, and stimulated healing. It was also proven that the periodontal attachment formation (alveolar bone, periodontal ligament-like tissue, and cementum-like tissue) was significantly increased compared to untreated scaffold [52]. The literature offers more studies on dogs, due to the greater ease with which each product can be put into practice and the higher number of tests. However, from a future perspective, the hydrogels developed in this work will be tested on cells derived from the dog's periodontium.

Lee *et al.* [62] fabricated graphene oxide (GO)-reinforced HAp/gelatin composite scaffolds by extrusion-based 3D-printing under precisely optimized printing parameters. The results showed that the proper addition of GO can efficiently reinforce the mechanical properties of HAp/gelatin composite scaffolds. Specifically, the compressive and flexural strength value of the HAp/gelatin composite scaffold was enhanced by 15% and 22% with the 0.5% GO incorporation, respectively. Based on the experimental results, this study suggests the great potential of using GO in the fabrication of composite bone scaffolds with improved mechanical properties for application in bone tissue engineering [62].

Park and his collaborators [47] studied the effect of bone morphogenetic protein (BMP) mimetic Peptide tethering bioinks on the differentiation of hDPSCs in 3D bioprinted dental constructs. They analyzed the properties of the bioink formulation and the stability of the bioprinted structure in order to be able to evaluate the survival and differentiation of hDPSCs in the construct. The study demonstrated successful peptide conjugation into the gelatin methacrylate-based bioink formulation. More than 50% of the peptides remained in the bioprinted construct after three weeks of *in vitro* cell culture. Human DPSC viability was over 90% in the bioprinted constructs immediately post-printing. The BMP peptide construct group exhibited significantly higher calcification compared to the growth medium, osteogenic medium, and non-BMP peptide construct groups, as demonstrated by the Alizarin Red staining results [47].

Chapter 3 - Materials and Methods

3.1. Materials

Gelatin type B was purchased from Acopharma (Spain). Glycerin (80 wt% pure) was purchased from Lacrilar (Portugal). Polyvinyl alcohol (PVA) a gift from Edol (Portugal). Betaine anhydrous was purchased from T. C.I. Europe (UK). Graphene Oxide (>95 wt% pure) was obtained from Graphenea (San Sebastian, Spain). Tannic acid and Ammonia solution (NH_4OH, 25%) were purchased from Sigma-Aldrich (Missouri, EUA). Citric Acid monohydrate ($C_6H_8O_7H_2O$, 99.5%) and Calcium nitrate tetrahydrate ($(Ca(NO_3)_2.4H_2O)$, 99%) were purchased from Riedel-deHaën (Germany). Ammonium hydrogen phosphate ($(NH_4)_2.HPO_4$, 99%) was purchased from Merck (Germany).

3.2. Preparation of Gelatin-based hydrogels' ink

The control formulation is the baseline for developing the final formulations with added active substances. Initially, the glycerin is added to 80% of the purified water total and taken to the bath at 75ºC, with the gelatin and PVA being added only after the mixture is at the right temperature. Once added, the formulation is left in the bath for 10 minutes until all the gelatin has dissolved. When this step is complete, the solution is placed in a water bath with constant magnetic stirring at the same temperature and the pH is adjusted to 8 using NaOH 1M. When the pH is equal to 8, TA is added, dissolved in 20% of the water total, drop by drop and intercalated with NaOH to ensure the stability of the pH at 8. After adding the TA, it is important to wait 1 hour for the reactions to take place. After this hour, the betaine is added, and the formulation is ready for printing.

3.3. Production of Hydroxyapatite nanoparticles

The hydrothermal method is a unique process for crystallizing substances from high-temperature (typically 100-250ºC) aqueous solutions at high vapor pressures [31] and is suitable for growing large nanoparticles while maintaining good control of the chemical composition. Figure 4 illustrates this process.

HAp nanoparticles were produced with citric acid monohydrate, ammonia solution, ammonium hydrogen phosphate and calcium nitrate tetrahydrate. An aqueous solution of 0.6M citric acid monohydrate was prepared with the requirement for pH adjustment to 8.1 by adding small

amounts of an ammonia solution. It is crucial that the pH is always measured before and after adding solutions. To that same solution, another solution of 0.2M ammonium hydrogen phosphate and an aqueous solution of 0.2M calcium nitrate tetrahydrate are added. During this process, the solution should be kept at pH=8.1 with a maximum temperature of 25°C. The solution was transferred into four 50 ml Teflon-lined stainless-steel autoclave, and they were sealed and heated at 180ºC for 24h. The precipitate HAp particles were obtained by filtration. After that, the solution was subjected to centrifugation for 3 minutes and then washed with distilled water several times. The products were stored in a desiccator.

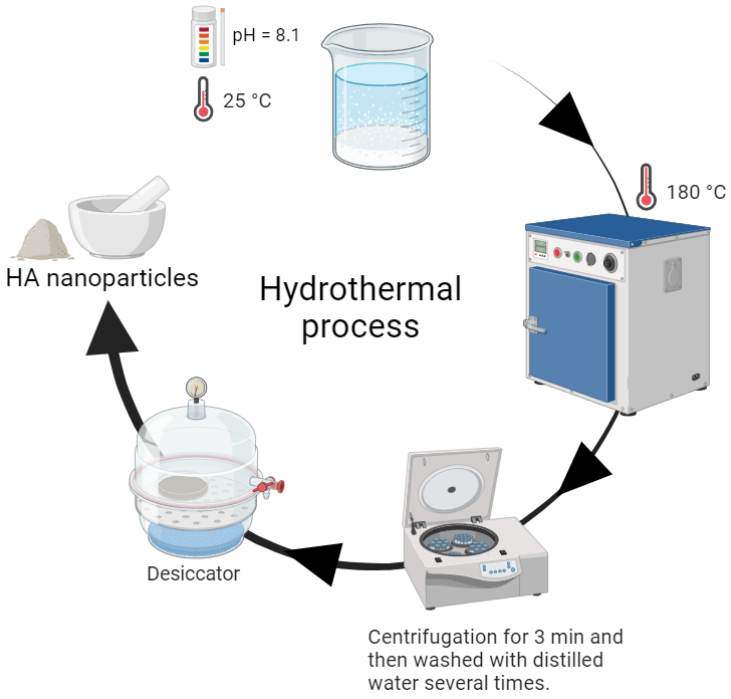

Figure 4 - Flowchart of the hydrothermal process.

3.4. Characterization of Hydroxyapatite nanoparticles

Transmission Electron Microscopy

Transmission Electron Microscopy (TEM) is an analytical technique to visualize the smallest structures in matter. TEM uses an electron beam emitted in the direction of the nanoparticle, providing higher resolution through light-based imaging techniques [63]. The interaction of the electrons transmitted through the NPs forms an image that is magnified and focused on an imaging device [64]. This technique provides information on morphology, structure, chemistry and type of bonds [65], being the preferred method to directly measure morphology and the size of nanoparticles [63].

TEM images of HAp nanoparticles were acquired using Hitachi Model H8100, at 200 kV, with LaB6 filament analytical transmission electron microscope (Thermo Fisher Scientific, Waltham, MA, USA).

3.5. Incorporation of compounds in control formulation

The formulations can be categorized as Group_GO37.5 and Group_GO7.5. Both groups contain formulations with equivalent gelatin quantities and active substances, differing only in the quantity and addition of glycerin.

In both groups, in addition to control, three more types of formulations were developed, where substances were added to the initial formulation – GO and HAp-NPs. These formulations follow the same procedure as the control, with both being incorporated at the beginning - In Group_GO37.5, the objective was to test the greatest possible quantity of GO by almost completely replacing the aqueous fraction with this component. Consequently, these preparations are designed to have a higher percentage of GO. In Group_GO7.5, the focus was on optimizing a formulation for printing without losing the beneficial characteristics of its components, maintaining a percentage of GO higher than HAp, in order to guarantee the desirable mechanical properties. Table 2 describes the composition of all formulations.

Table 2 - Qualitative and quantitative composition of all formulations.

	Ink Formulation	Gelatin (%)	Glycerin (%)	PVA (%)	Betaine (%)	TA (%)	GO (%)	HAp-NPs (%)	H_2O (%)
Group_GO37.5	GEL30	30	-	1.5	3	0.9	-	-	64.6
	GEL30-GO37.5	30	-	1.5	3	0.9	37.5	-	27.1
	GEL30-HAp0.1	30	-	1.5	3	0.9	-	0.1	64.5
	GEL30-GO37.5-HAp0.1	30	-	1.5	3	0.9	37.5	0.1	27
Group_GO7.5	GEL30	30	10	1.5	3	0.9	-	-	54.6
	GEL30-GO7.5	30	10	1.5	3	0.9	7.5	-	47.1
	GEL30-HAp2	30	10	1.5	3	0.9	-	2	52.6
	GEL30-GO7.5-HAp2	30	10	1.5	3	0.9	7.5	2	45.1

3.6. Characterization of Gelatin-Based Hydrogels

3.6.1. Rheological characterization

Temperature sweep tests with oscillatory shear were performed with a stress Kinexus Lab+ Rheometer (Malvern Instruments, Malvern, UK). The measurements were carried out with a plate–plate geometry and a gap of 0.5 mm (patch height simulation). The onset of gelation

temperature was defined as the crossover (G′ = G″). All measurements were performed from 75°C to 25°C at a rate of 2.5 ºC/min; frequency was kept at 1 Hz and the shear strain at 1%.

3.6.2. ATR-FTIR Spectroscopy

Attenuated total reflectance (ATR) is often used with Fourier transform infrared (FTIR) spectroscopy (ATR-FTIR). ATR is a sampling technique that uses total internal reflection to generate an evanescent wave that penetrates the membranes, providing valuable molecular information, in order to identify chemical compounds, molecular structures, examining surface properties and analyzing polymers [59, 60]. This methodology allows the direct examination of solid or liquid samples without further preparation. In ATR-FITR, light energy is passed through an optical material that must be optically transparent to the frequency of the energy [66]. It is based on infrared light absorption in the wavelength range of 2.5-25 μm by the material, resulting in the occurrence of a mechanical motion of different forms with the molecule or compound atoms [68].

To identify the functional groups of the patches from Group_GO37.5 (4 membranes) and Group_GO7.5 (4 membranes), ATR-FTIR spectra were acquired using a Nicolet FTIR spectrometer (Thermo Electron, Thermo Fisher Scientific, Waltham, MA, USA). The hydrogel's membranes and HAp nanoparticles were placed on the ATR diamond crystal, and spectra were obtained in the range of 500 to 4500 cm^{-1} with a resolution of 8 cm^{-1}. The recorded signals were reported as transmittance.

3.6.3. Scanning Electron Microscopy

Scanning Electron Microscopy (SEM) is an advanced imaging technique that uses electrons instead of light and is employed to acquire a high-resolution view of membranes surfaces. SEM uses the electrons that are reflected or knocked off the near-surface region of the sample to create an image. This technique presents higher resolution due to the wavelength of electrons being much smaller than the wavelength of light electrons [69].

The morphology of the hydrogel membranes as well as the distribution and size were examined using a scanning electron microscope (SEM Hitachi S2400, Tokyo, Japan).

3.6.4. Energy Dispersive Spectroscopy

Energy Dispersive Spectroscopy (EDS) technique is most used for qualitative analysis of materials, however, is also capable of providing semi-quantitative results. The SEM equipment

has an EDS system enabling the chemical analysis of observed features on the SEM display. Simultaneous SEM and EDS analysis is crucial in scenarios where spot analysis is necessary to obtain valid conclusions during failure analysis. The signals generated within a SEM/EDS include both secondary and backscattered electrons, employed for morphological analysis to form images, and X-rays, applied the identification and quantitative analysis of chemicals present at detectable concentrations. The detection limit of EDS is contingent upon the surface conditions of the membrane, with smoother surfaces correlating to lower detection limits. EDS exhibits the capability to discern major and minor elements at concentrations exceeding 10 wt% for major elements and within the range of 1-10 wt% for minor elements. This technique is capable of producing elemental distribution maps [68].

This method was used to confirm the presence of HAp and to analyze the distribution of components in the gelatin-based membranes. The results were acquired from scanning electron microscope with Bruker Quantax energy dispersive X-ray spectrometer (SEM Hitachi S2400, Tokyo, Japan).

3.6.5. Water Stability

The trials were carried out with membranes stored at 4ºC and 25ºC, to understand whether temperature affected their absorption capacity. To test its water-absorption capacity, a membrane of each formulation was placed in 2 ml of purified water one day after it was produced. This test was performed at 25ºC and 37ºC (body temperature) over 7 hours. The membranes were weighed before the test (Wi) and at the end of the test (Wf).

The water absorption capacity was calculated according to the following equation (1):

$$Water - absorption\ capacity\ (\%) = \frac{Wf - Wi}{Wi} \times 100 \qquad \textbf{(1)}$$

3.6.6. Degradation Ratio

The degradation ratio of the membranes with different drying times (i.e. 1, 2, 7 and 15 days) were measured through immersing the membranes in 5 ml of Phosphate Buffered Saline (PBS) each and storing them in an incubator at 37°C. The initial weights of the membranes (n=3) were weighted (Wi), lodged in 6-multiwell tissue culture polystyrene (TCPS), immersed in 5 mL PBS (pH=7.4), stored at 37 °C and weighted at established time points (Wt) up to 21 days. At certain time intervals (1, 7, 15 and 21 days), membranes were taken out and their weights were recorded after excess water was removed. The weight ratio of each membrane

at a specific weight (Wt) in relation to the initial weight of the dry membrane was monitored as a function of the immersion time. The measurements were performed until the complete collapse of the membranes. The longer the drying period post-production, the higher the level of resistance to degradation it will exhibit over time.

The degradation ratio was calculated according to the following equation (2):

$$Degradation\ Ratio\ (\%) = \frac{Wi - Wt}{Wi} \times 100 \quad \textbf{(2)}$$

3.6.7. Tensile Tests

Tensile testing is a destructive material science and engineering technique in which controlled tension is exerted on a membrane until it reaches complete failure. The test serves as a form of tension testing, adhering to rigid standards, and requires precise instrumentation [70, 71]. Figure 5 demonstrates the specimen used in the tensile tests.

This test involves a membrane held in two grips a set distance apart and it measures the force required to break a composite or plastic specimen and the extent to which the specimen is stretched or elongated to the breaking point [72].

Tension tests were performed in accordance with specimen geometry standard ISO 527 (Figure 5). The area of the cross-sectional zone was calculated as shown in Figure 6, with the multiplication of specimen width (W) by the length (l). F is the load applied by the texture analyzer.

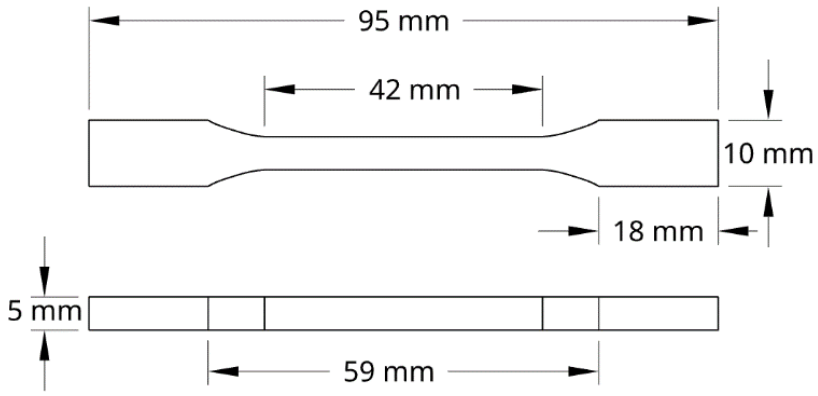

Figure 5 - Specimen geometry and measurements used in tensile tests.

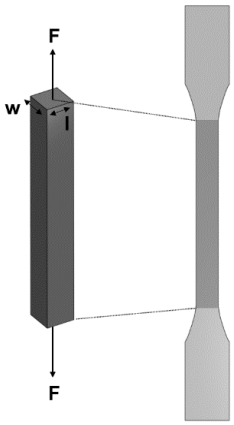

Figure 6 - Diagram explaining the cross-sectional area of the specimen.

The stress was obtained using equation (3):

$$Stress\ (KPa) = \frac{\text{Force (N)}}{\text{Area (m}^2\text{)}} \quad \textbf{(3)}$$

The results were acquired from TA.XTplus texture analyser (Stable Micro Systems, UK) equipped with 30kg of load cell, operated at 0.5 mm/sec was employed to evaluate tensile properties. Specimens were mounted into the load frame and held by the appropriate load cell.

3.7. 3D Printing

The printing conditions were tested using various codes, in *G-code* format, previously developed. To generate all the codes used in this study, firstly the software *onshape* was used to design the desired shape and then it was loaded into the CURA software to define the printing characteristics applied to the printer.

The 3D printer used in this project was *Allevi* 2 (3D Systems, California, EUA) – Figure 7.
It has two extruders and is built around a compressed air pneumatic system and the pressure ranges between 1 and 120 Psi, functioning to a wide range of viscous materials.

The temperature control can be set from room temperature to 160ºC, being able to print numerous types of inks, including gelatin, Polycaprolactone and poly(lactic-co-glycolic acid). The printer offers photocuring, allowing users to select visible or ultraviolet light to cure biomaterials with LAP or other photo initiators [73].

Figure 7 - *Allevi* 2 [73].

3.7.1. Line test

To determine the optimal printing speed, a line test was conducted comparing three different speeds (10mm/sec, 20mm/sec, and 30mm/sec) with the nozzle used. Linear filaments with 40mm were printed under specified temperature and pressure conditions at printing speeds ranging from 10 to 30 mm/s (n=3 per condition) to analyze the impact of these parameters on filament width (W') and length (L') index measurements. The L' was obtained by dividing the length of the printed filament by the length of a theoretical, perfectly uniform strand, as shown in equation (4):

$$L'\ (\mathrm{mm}) = \frac{\text{Printed filament lenght}}{CAD\ filament\ lenght} \quad \textbf{(4)}$$

W' is responsible for analyzing the extent to which the filament spreads laterally and can be calculated using equation (5):

$$\mathrm{W}'\ (\mathrm{mm}) = \frac{\text{Printed filament width}}{\text{Needle diameter}} \quad \textbf{(5)}$$

The measurement of filament width and length (n=3) was conducted using the ImageJ software.

3.7.2. Printing parameters

The printing process occurred after the production of the ink at the temperature of 75ºC. The cartridge was pre-heated at 40ºC, and, after that, the gelatin-based hydrogel inks were transferred to the inside of the cartridge. Due to the temperature differential, it is essential to allow approximately 30 minutes for the formulation to reach the desired temperature. The inks were extruded through specific nozzles, Figure 8, with 27 Gauge and an inner diameter of

0.335 mm (pink metal tip) and 25 Gauge with an inner diameter of 0.435 mm (white metal tip), depending on the ink composition. Through rheology studies, it is possible to understand that inks with GO in their composition need a larger inner diameter, due to higher viscosity. The pink metal tip with a smaller inner diameter was chosen for both the control gelatin-based hydrogel and control with HAp-NPs. This selection was due to the lower viscosity of this type of ink.

After the stabilization, filament tests were performed to analyze if the filament extrusion was made with proper gelation. The conditions are tested through a standing extrusion, to make sure that the printing occurs without any issues (nozzle clogging or gelation of the formulation).

Figure 8 – Nozzles used for printing the 3D hydrogel inks. The pink and white nozzles are metal tips with 27 Gauge and 25 Gauge, respectively. Pictures retrieved from [73].

To enhance the effectiveness of substances' release and facilitating the diffusion of nutrients and oxygen from the 3D membrane, it is crucial to establish porosity. For this purpose, three layers were created with distinct orientation angles (1st layer 45º, 2nd layer 90º and 3rd layer 135º respectively). All the layers were printed with a 0.15 mm layer height, 0.6 mm line width and 30 mm/s printing velocity and were maintained constant for every ink. An illustration of the designs can be seen in Figure 9. The optimized printing parameters used for each gelatin-based hydrogel ink is described in Table 3.

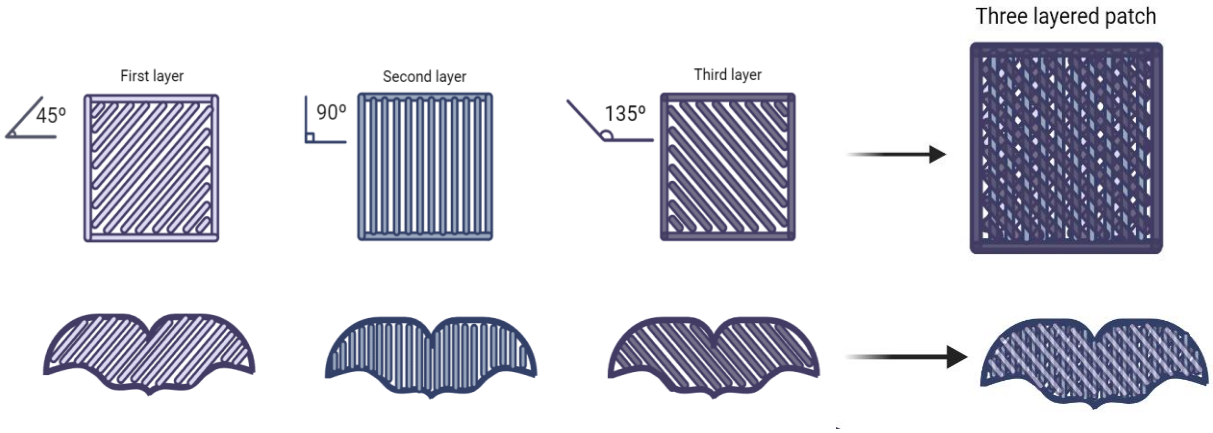

Figure 9 - Illustration of two designs produced. The three layers individually and the final three-layered patch. The first, second and third layers have an angle of 45°, 90°, 135°, respectively. All layers were printed with 0.15 mm layer height, 30 mm/s printing velocity and 0.6 mm.

Table 3 - Printing parameters used in all gelatin-based hydrogel formulations.

Ink Formulations	$T_{Chamber}$ (ºC)	$T_{Cartridge}$ (ºC)	Pressure (Psi)	Printing velocity (mm/s)	Layer Height (mm)	Line Width (mm)
GEL30	25	40	15	30	0.15	0.6
GEL30-GO7.5	25	45	15	30	0.15	0.6
GEL30-HAp2	25	40	15	30	0.15	0.6
GEL30-GO7.5-HAp2	25	45	15	30	0.15	0.6

Chapter 4 – Results and Discussion

4.1. Characterization of Hydroxyapatite nanoparticles

Functional groups associated with hydroxyapatite nanoparticles (HAp-NPs) were identified by Attenuated Total Reflectance Fourier-Transform Infrared spectroscopy (ATR-FTIR) demonstrated in Figure 10.

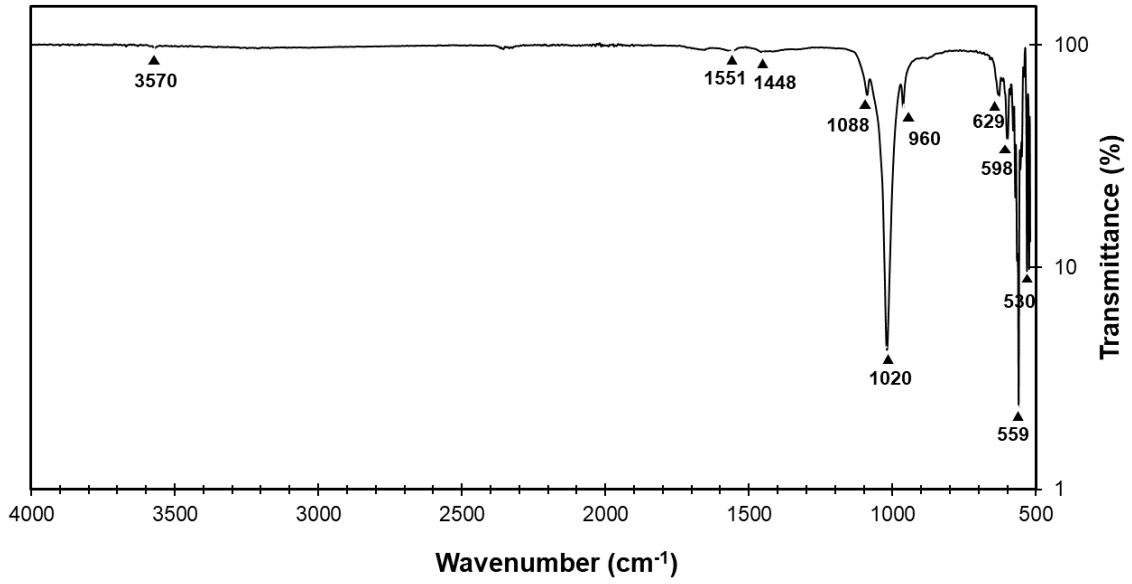

Figure 10 - ATR-FTIR spectrum of hydroxyapatite nanoparticles.

The analysis identified characteristic bands at 960 cm-¹, 1020 cm-¹ and 1088 cm-¹, corresponding to the stretching vibrations of the phosphate groups (PO_4^{3-}). Additionally, bands observed around 530 cm-¹, 559 cm-¹, 598 cm-¹, and 629 cm-¹ can be attributed to the bending vibrations of the P-O bonds in the phosphate groups. Peaks with decreased intensity were also found at 1551 cm-¹ and 1448 cm-¹ that corresponded to carbonate group (CO32-) [74]. As a result, the presence of the PO_4^{3-} group in hydroxyapatite is confirmed through ATR-FTIR studies. Additionally, there were peaks of decreased intensity detected at approximately 3570 cm-¹, indicating the existence of O-H bonds [74]–[77].

The synthesis process has a direct impact on the morphology of nanoparticles. The literature reports that when the nanoparticles are produced by the hydrothermal method at a temperature of 180ºC, they are expected to be in the form of nanorods [57, 79]. To determine the produced nanoparticles' morphology, TEM was conducted (Figure 11).

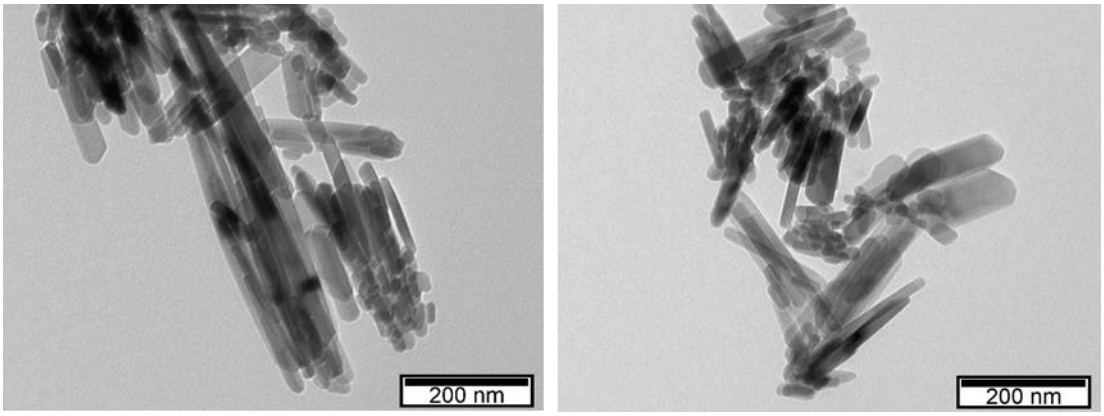

Figure 11 - Transmission Electron Microscopy images of hydroxyapatite nanoparticles.

The TEM images confirmed the nanorod morphology and present a smooth surface morphology. Aggregations of particles can be observed. Due to this type of synthesis being slower, the nanoparticles grow with more defined forms.

4.2. Characterization of Ink Formulations

4.2.1. Rheology Properties

The study of rheology is a crucial factor in understanding the behavior of the formulations being developed. To achieve precise 3D-printed structures, the multimaterial formulation's printing parameters were optimized by conducting rheological and printability assessments. Properly optimizing printing parameters and conducting a rheological analysis of the composite is crucial since each parameter, including printing temperature, extrusion pressure, and printing velocity, is greatly influenced by the rheological properties of the printing material [62].

Therefore, it is important to analyze the relation between G' and G'' and identify the crossover point that provides the hydrogel's gelling point. This point is the instant when the elastic and viscous moduli equalize, indicating a change in the material's response from predominantly elastic to predominantly viscous behavior. The value of the gelling point will provide information on the temperature at which the extrusion of the material into the print will be more stable and more precise. Achieving a proper balance between viscous and elastic modulus is necessary to ensure high printing accuracy and shape fidelity [79]. The onset of gelation temperature was obtained when the shear storage modulus G' is equal to the loss modulus G" (G′ = G″).

The study began by testing four different formulations from Group_GO37.5, including a control with a gelatin base of 30%. One formulation included the addition of 37.5% GO (GEL30-GO37.5), and another had 0.1% HAp (GEL30-HAp0.1). A final formulation was analyzed that had both active substances (GEL30-GO37.5-HAp0.1). The results of all formulations are displayed in Figure 12, which shows the relationship between temperature and the values of G' and G".

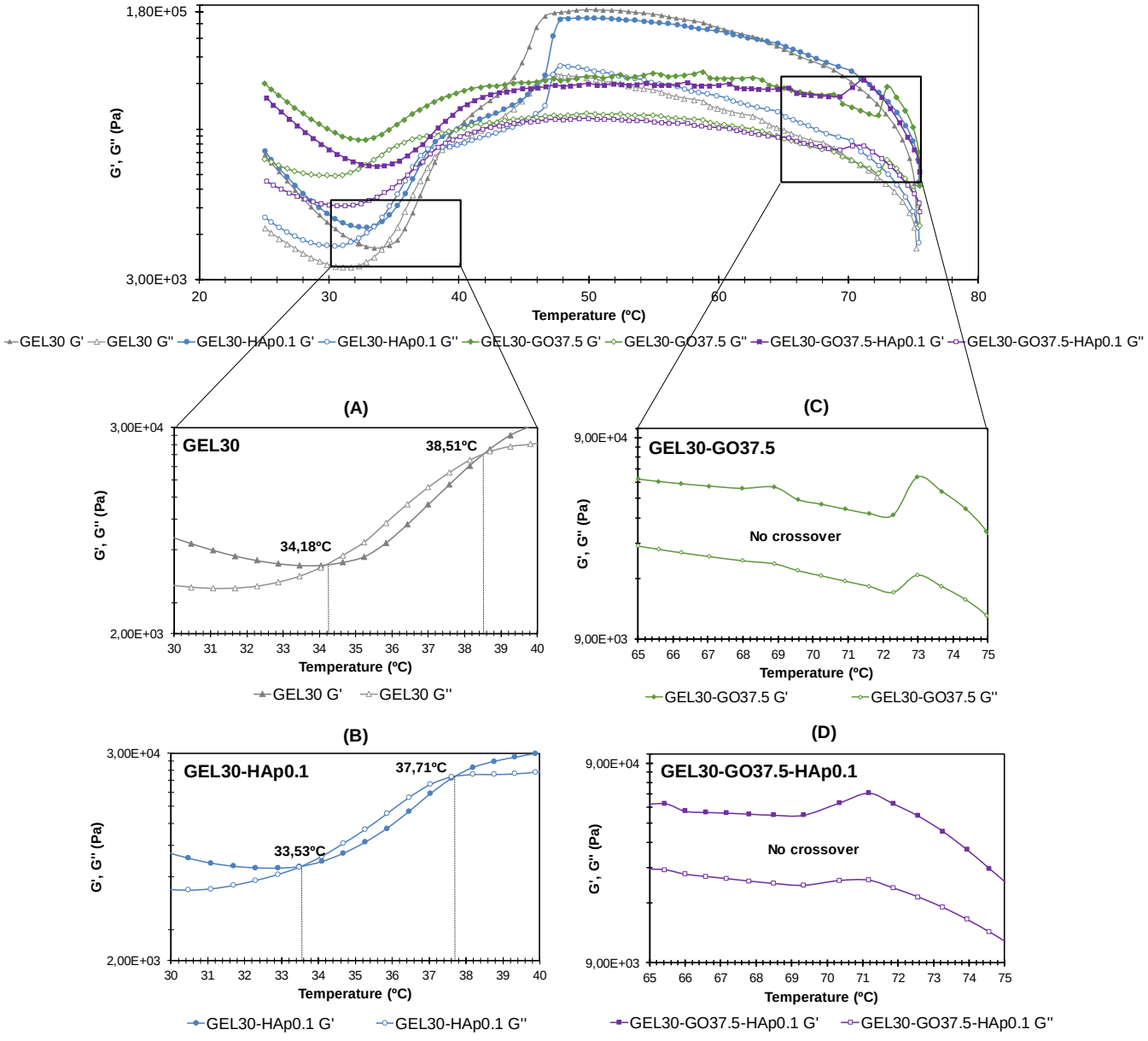

Figure 12 - Rheological temperature sweep of gelatin-based formulations – Group_GO37.5. (A) GEL30 (Control formulation). (B) GEL30-HAp0.1. (C) GEL30-GO37.5. (D) GEL30-GO37.5-HAp0.1.

Considering the graph with all the multimaterial formulations, it is immediately noticeable that all the G' values are significantly higher than G''. This graph highlights the similarities between formulations containing GO. Following this, GEL30-GO37.5 and GEL30-GO37.5-HAp0.1 start with low values of G' and G'' and significant oscillations up to 60ºC. From this point, a nearly constant behavior can be observed between temperatures of 60ºC and 40ºC. This behavior exhibits stability within this temperature range, justified by the fact that all formulations are produced at 75°C, where they are at their most fluid. It is important to find a balance between G' and G'' - ideally until they are equal - because even though the formulations have very low values at 75ºC, they are too fluid to print and do not meet the requirements for precise print stability. Upon cooling to ambient temperatures, both moduli increase again. GEL30 and GEL30-HAp0.1 begin with low values of G' and G'', but continue to increase, except when approaching a temperature close to 40ºC, down to 34ºC. However, it is clear from this graph that G' is significantly higher than G'' in all formulations, proving that it behaves in an elastic behavior, which is a disadvantage for 3D printing [31].

Figure 12 demonstrates the similarity in behavior between GEL30 (Figure 12A) and GEL30-HA0.1 (Figure 12B), despite the insignificant amount of HAp added. It is notable that even small amounts of HA prompted a slight decrease in the temperature of the gelling points of GEL30-HAp0.1 compared to GEL30. Figure 12C, GEL30-GO37.5 and Figure 12D, GEL30-GO37.5-HAp0.1 formulations, displays no crossover point, indicating that these composites does not experience a viscoelastic shift that defines the establishment of a gel structure as temperature increases. Instead, these formulations maintain their elastic nature throughout the temperature range considered, without forming a gelatinous structure.

If a crossover point is not observed, this may indicate that the material does not have the specific phase transition properties typical of thermoreversible gels and, if applied to 3D printing, would be very complicated and challenging to achieve the printing parameters needed to extrude accurately.

To demonstrate the significance of this variable in printing, viscosity through temperature was analyzed in Figure 13A. This figure demonstrates that as temperature decreases, the viscosity increases, creating a more difficult printing process, even in the most stable range. Figure 13B illustrates the extrusion of GEL30-G037.5-HAp0.1 at 50ºC, a temperature chosen from the most stable range, where it is possible to observe a gelled and heterogeneous droplet, incapable of forming continuous homogeneous filaments. The printing strand tests were not conducted at 75°C since this temperature represents the point at which the formulation is the most fluid due to its production temperature. At such a fluid state, the formulation lacks the consistency required to produce filaments that are resistant to deformation.

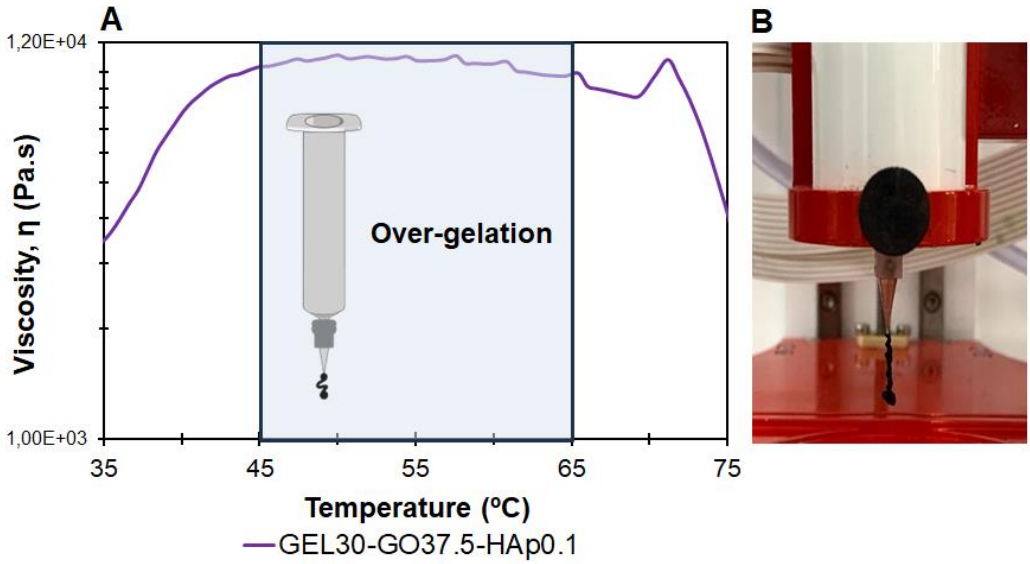

Figure 13 - The role of viscosity in printing process. A - Analysis of viscosity with temperature. B - Strand test showing over-gelation through printing at 50ºC.

To comprehend how the active substances affect the base's viscosity, an isothermal analysis was conducted on the behavior of GEL30-GO37.5-HAp0.1 at its production temperature (75ºC) over time for 6 hours (Figure 14).

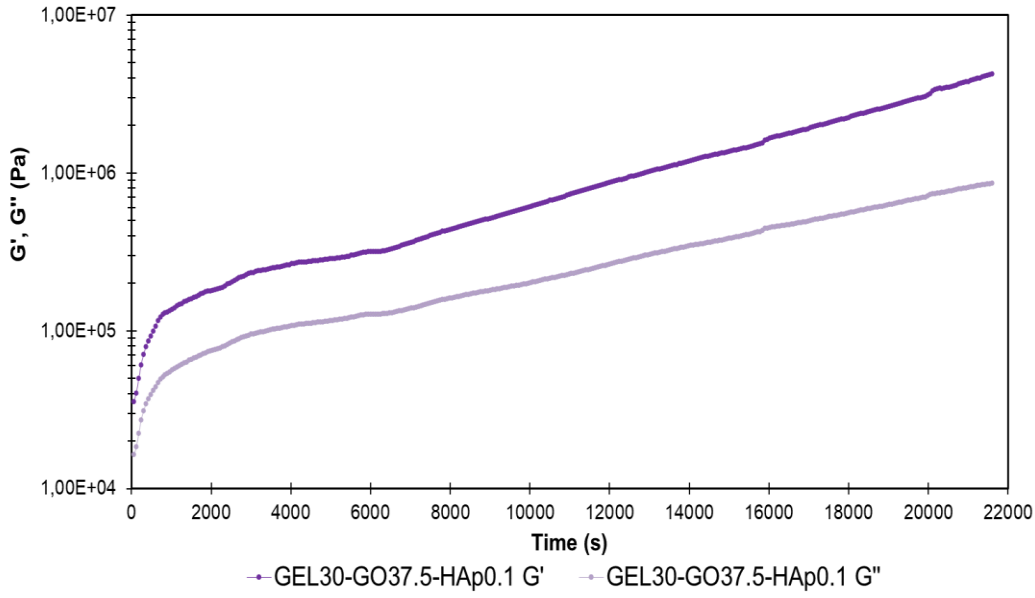

Figure 14 - Isothermal analysis on GEL30-GO37.5-HAp0.1.

Isothermal analysis is conducted at a constant temperature without any thermal variation over time. This analysis is crucial in determining a system's equilibrium behavior, thermal stability, and phase transitions at a specific temperature. According to Figure 14, as the G' and G'' modules increase, the viscosity of the formulation increases over time. This confirms that the

gel is undergoing solidification, leading to a rise in the material's stiffness as demonstrated by the G' and G'' moduli. The process may be driven by the gradual loss of water concentration over time, resulting in higher levels of solids in the formulation. Another contributing factor is the presence of GO, which accelerates the reactions between different components.

These results confirmed that when GO is utilized as a reinforcement, its addition in substantial quantities is believed to enhance the elastic behavior of the formulation, thereby improving the mechanical properties of the hydrogel [80]. Meanwhile, HAp nanoparticles, when incorporated in small amounts, have no significant effect on the behavior of the formulation.

After analyzing the results, it became evident that the previous quantity of GO implemented was excessive for the desired outcome. Consequently, alternative formulations were developed (Group_GO7.5) and tested once more under identical conditions to determine the optimal amount required. The goal of producing new formulations was to obtain rheological characterization curves that would be advantageous for printing, while still providing the properties required for the multimaterial formulation purpose. Consequently, the amount of GO was decreased to 7.5% and HAp was increased to 2%. Additionally, 10% glycerin was added, a well-known material used in printing as a plasticizer [81], wetting agent [5,6] and surface tension reducer [83]. The rheological characterization of these formulations from Group_GO7.5 can be observed in Figure 15.

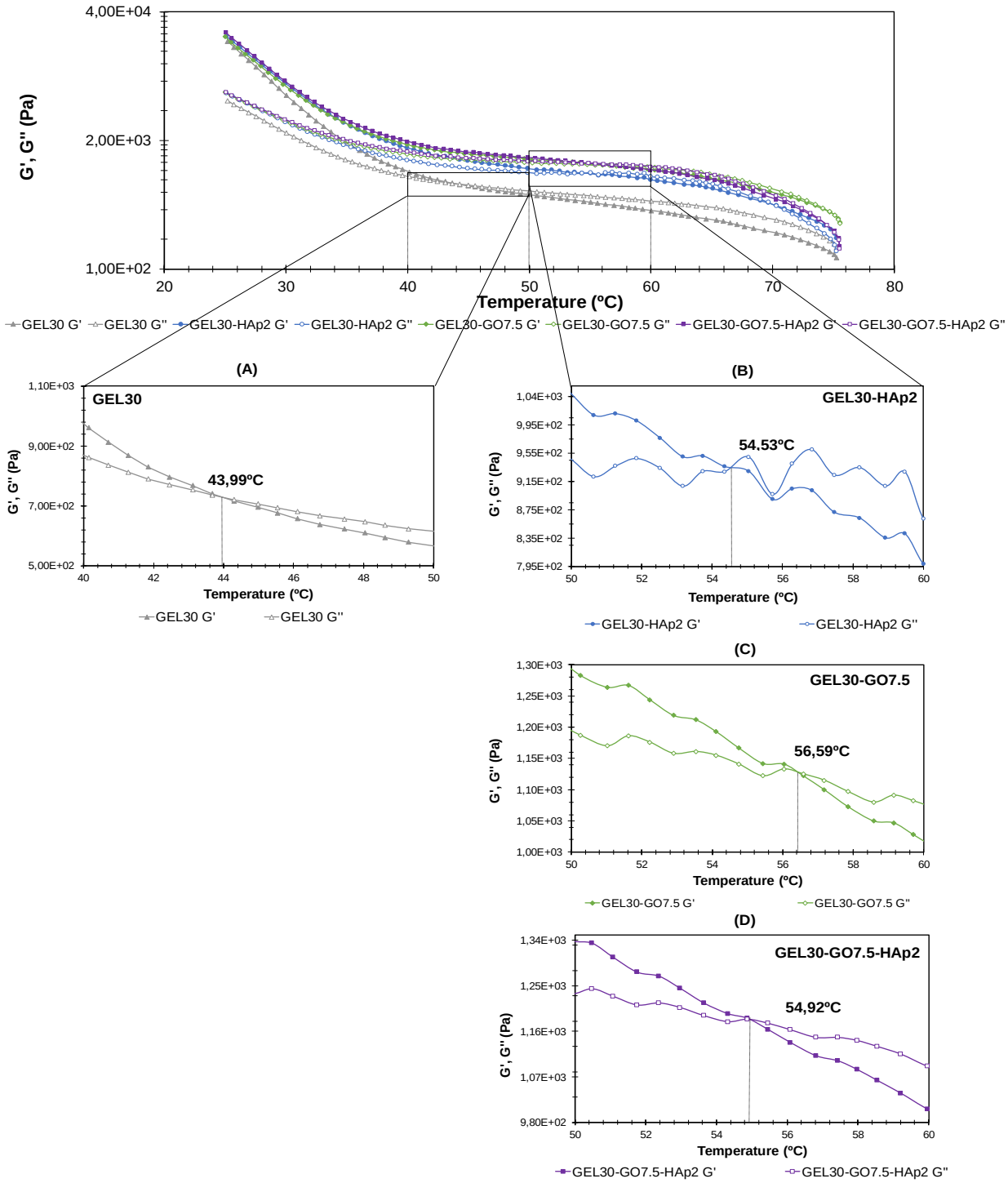

Figure 15 - Rheological temperature sweep of gelatin-based formulations – Group_GO7.5. (A) GEL30 (B) GEL30-HAp2. (C) GEL30-GO7.5. (D) GEL30-GO7.5-HAp2.

Based on Figure 15, all multimaterial formulations share the identical principle, and display comparable features. The G'' modulus initially exhibits higher values than the G' modulus at a temperature of 75ºC. This process reverses only after reaching the gelling point, as expected. These fluids exhibit an expected behavior of having a lower viscosity at 75ºC (production

temperature) and increasing all the way to values close to room temperature. An optimal printing formulation is expected to undergo an increase in viscosity as temperature decreases. Figure 15A displays the control formulation, demonstrating stable behavior and a gelling temperature of approximately 44ºC, with lower viscosity values than all other formulations, as expected. Upon the addition of HAp nanoparticles, shown in Figure 15B, the gelling temperature increases by 10ºC. At this point, the G' and G'' increases from 7.28E+ 02 Pa to 9.35+ 02 Pa compared to the control. These results indicate that the small percentage of HAp nanoparticles added does not significantly alter the behavior of the formulation but affects the temperature. When analyzing GEL30-GO7.5 (Figure 15C), GO can be seen to increase G' and G'' from 7.28E+ 02 Pa (GEL30) to 1.13E+ 03 Pa, despite the lower percentage used compared to previous trials. The increase is due to the mechanical characteristics of GO, which increase material rigidity. Concerning the formulation with all substances added (GEL30-GO7.5-HAp2), which can also be seen in Figure 15D, the values of G' and G'' are 1.18E+03 Pa and the gelling temperature is approximately 55ºC. Comparing this outcome with the formulations containing HAp and GO individually, the presence of both components in the same formulation increases the gelation temperature and viscosity at the same point. In this scenario, GO played a more significant role in enhancing viscosity due to its higher concentration compared to HAp.

The viscosity versus temperature study was also performed to demonstrate the different types of scenarios that exist in the 3D printing process in relation to temperature variation. Figure 16 illustrates the three gelation types identified for the viscosity values of the GEL30-GO7.5-HAp2 formulation.

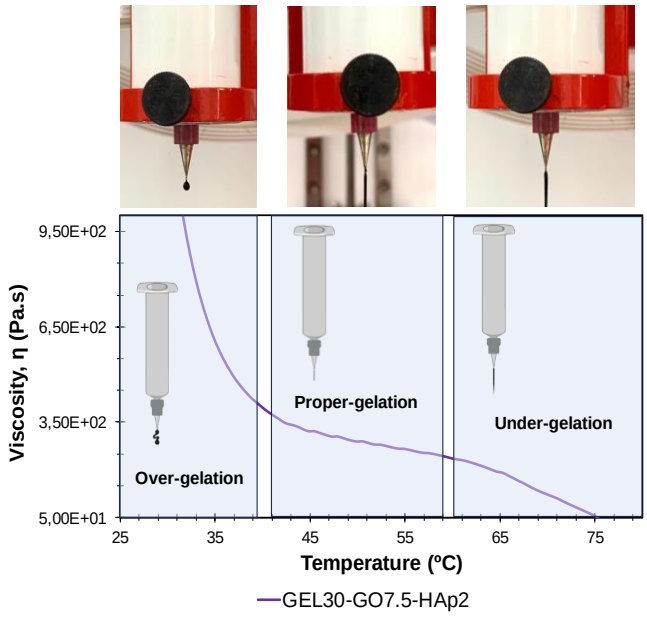

Figure 16 - Analysis of viscosity with temperature. The three types of gelation identified in GEL30-GO7.5-HAp2.

At high viscosity, the GEL30-GO7.5-HAp2 becomes gelled and is unable to extrude through the nozzle. At low viscosity - at temperatures closer to 75ºC - the formulation becomes very fluid, preventing the formation of a consistent filament. The proper-gelation is observed nearer to the temperature of gelation.

The gelation temperature values (Sol-gel temperature), as well as the viscosity and G* complex values at this temperature for all formulations, are detailed in Table 4.

Table 4 - Rheological parameters of all final formulations.

Formulations	Rheological parameters		
	Sol-gel temperature (ºC)	G* at sol-gel (Pa)	Viscosity at sol-gel (η, Pa.s)
GEL30	54.53	1321	209.9
GEL30-HAp2	43.99	1030	163.9
GEL30-GO7.5	59.59	1589	252.8
GEL30-GO7.5-HAp2	54.92	1674	266.5

Studies on gelatin-based formulations support viscosity values of approximately 200 Pa.s for stable and accurate printing [31]. In these formulations, active substances are added, which always increases their viscosity compared to gelatin-based formulations without the addition of components with similar properties. Formulations containing GO exhibit higher viscosity than control formulations or only HAp, justifying the role of GO in increasing viscosity.

4.3. Characterization of Gelatin-based Hydrogels

The only hydrogels that will be studied in this chapter, after 4.3.1, are from Group_GO7.5, since they have shown the best rheological results, and they are going to be used in the 3D printing process.

4.3.1. The effect of the addition of HAp and GO to the hydrogel

Functional groups associated with the compounds used in gelatin-based hydrogels were identified by Attenuated Total Reflectance Fourier-Transform Infrared spectroscopy (ATR-FTIR) demonstrated in Figure 17. This analysis enabled understanding of the effect of the nanoparticles on the hydrogel.

Group_GO37.5 shares identical active substances with Group_GO7.5 but does not contain glycerin. Moreover, the order of addition differs in Group_GO37.5, where PVA and betaine are added at the end. Group_GO37.5 is distinguished by containing high proportions of GO and low amounts of HAp in its formulations.

Upon analyzing all 4 hydrogels, a comparable structure was detected in each of them, proving that there are no chemical changes when all components are present. It is anticipated that characteristic bands of the predominant compounds (Gelatin, PVA, TA and GO) will be identified. All structures were detected by the dashed lines.

The FTIR spectra (Figure 17) indicates the presence of absorption bands characteristic of peptide bonds, present in gelatin: Amide A, I and II. Amide A is one of the most important structural groups in gelatin and appears in a broad band at ~3301 cm^{-1} demonstrated by Skopinska-Wisniewska *et. al* [84], due to N-H stretching vibrations. In this figure, the peak 3325 cm^{-1}, in all formulations, is characteristic of Amide A. Another group of gelatin is Amide I (~1635 cm^{-1}), induced by C=O stretching vibrations; and Amide II (1562 cm^{-1}), caused by the bending vibrations of N–H groups and stretching vibrations of C–N groups [85].

Peaks with decreased intensity were identified at 1562 cm^{-1} that could correspond to the deformation vibration of C-H and it is often associated with the bending of methylene (CH_2) groups in the polymer backbone of PVA [86]. The 1635 cm^{-1} peak can also correspond to the deformation vibration of −OH of the carboxyl group due to the presence of −COOH in PVA [87] or to ester C=C aromatic bond stretching, characteristic of TA's spectrum. The analysis identified a peak of decreased intensity at 2357 cm^{-1} corresponding to carbon-carbon triple bond (C≡C) in compounds such as alkynes. This can be justified by the presence of sodium hydroxide (NaOH). No TA, HAp or GO absorption bands can be observed in this analysis.

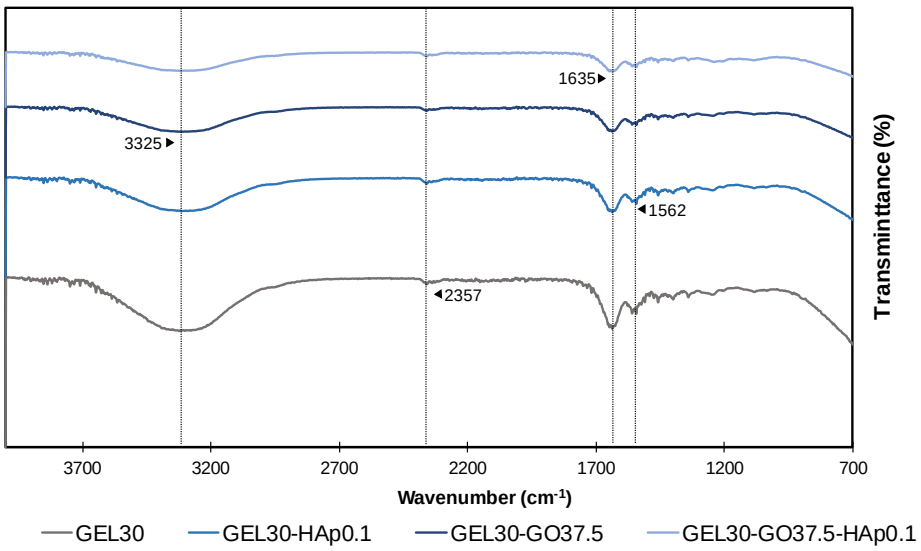

Figure 17 - ATR-FTIR spectrum of Group_GO37.5 gelatin-based hydrogels.

Group_GO7.5 is distinguished by containing lower proportions of GO and higher quantity of HAp, compared to Group_GO37.5, in its hydrogels.

As observed in Group_GO37.5, this group exhibits very noticeable similarity between all its hydrogels, which proves that there are no chemical changes when all the components are combined. The analysis identified characteristic band from gelatin at 3278 cm^{-1}, as expected. Amide A bands appear in a broad band at ~3301 cm^{-1}. The difference can be justified due to the water content of the membranes, that provokes a OH stretching band in this area [85].

Peaks with decreased intensity were detected at 2949 cm^{-1} due to aliphatic C-H stretching vibrations present in PVA and Gelatin [88]. Such as Group_GO37.5, the peak identified at 1562 cm^{-1} could correspond to the deformation vibration of C-H and it is often associated with the bending of CH_2 groups in the polymer backbone of PVA [86]. The peak at 1635 cm^{-1} was accredited to ester C=C aromatic bond stretching, characteristic of TA's spectrum [88] or can also correspond to the deformation vibration of −OH of the carboxyl group due to the presence of −COOH in PVA [87].

The peak at 1234 cm^{-1} and 1034 cm^{-1} corresponds to C-O and aryl oxygen stretching, respectively [19, 20].

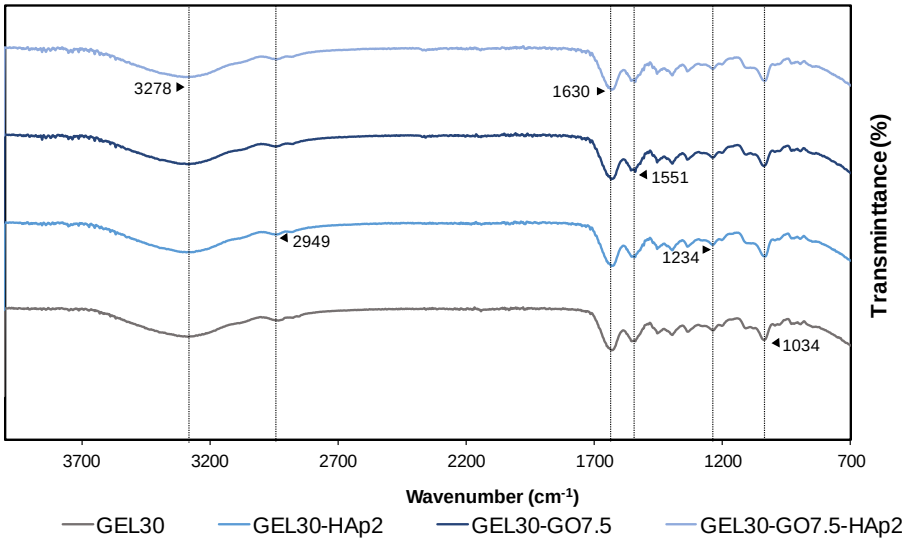

Figure 18 - ATR-FTIR spectrum of Group_GO37.5 gelatin-based hydrogels.

Both Group_GO37.5 and Group_GO7.5 exhibit bands indicative of PVA, TA, and gelatin. No peaks representative of GO or HAp are present, as the method of analysis was incapable of detecting the specific functional groups.

The SEM images of the surface of the four multimaterial gelatin-based hydrogels is demonstrated in Figure 19.

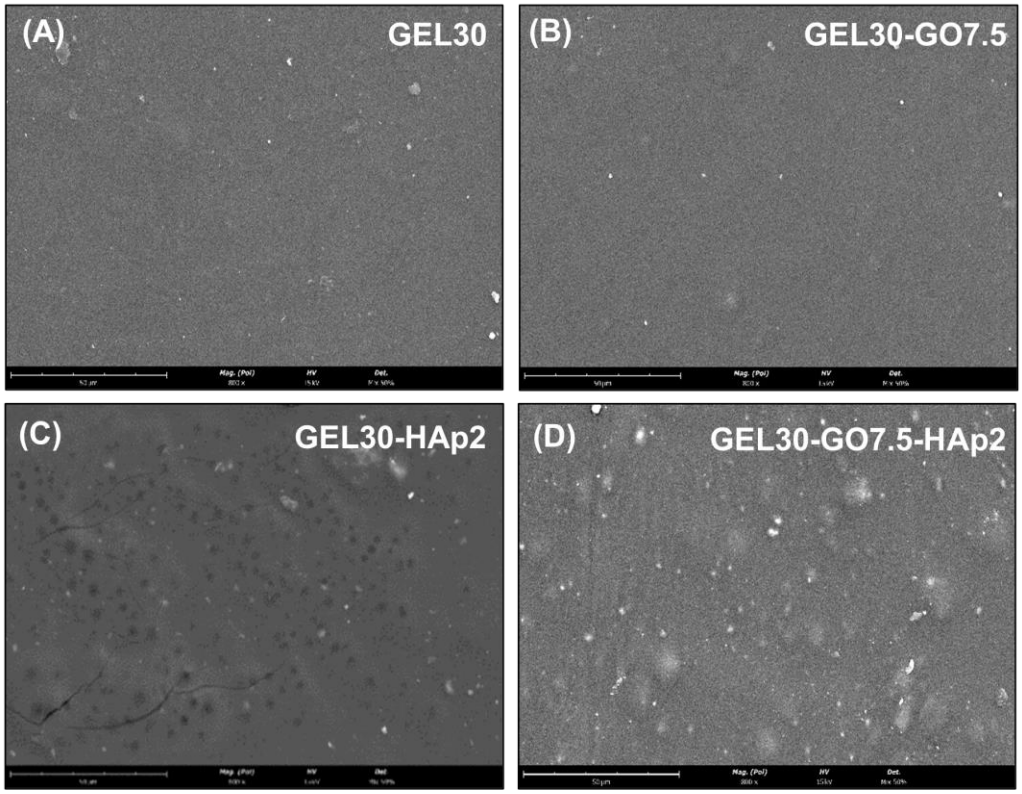

Figure 19 - SEM images of Group_GO7.5 gelatin-based hydrogels. (A) GEL30, (B) GEL30-GO7.5, (C) GEL30-HAp2 and (D) GEL30-GO7.5-HAp2.

The surfaces of GEL30 (Figure 19A) and GEL30-GO7.5 (Figure 19B) hydrogels both exhibit homogeneous distributions of their components. GO is imperceptible in any hydrogel due to its uniform nanoparticle dispersion without agglomerations. Various clusters of HAp nanoparticles are visible from the surfaces of GEL30-HAp2 (Figure 19C) and GEL30-GO7.5-HAp2 (Figure 19D) membranes.

EDS was performed to analyze the quantification of the constituent elements of HAp (phosphate and calcium) and GO (carbon and oxygen) present in GEL30-HAp2 (Figure 20) and GEL30-GO7.5-HAp2 (Figure 21) hydrogels and their distribution. The SEM image of the multimaterial GEL30-HAp2 hydrogel is shown in Figure 20A. Figure 20B and Figure 20C demonstrates the presence of calcium and phosphate in hydrogels' surface, respectively. Figure 20D exhibits the Energy dispersive X-ray spectroscopy (EDXS) spectrum of the hydrogel, from a specific white cluster (indicated in Figure 21A), making it is possible to observed that HAp is present. Table 5 demonstrates the Ca/P ratio in GEL30-HAp2.

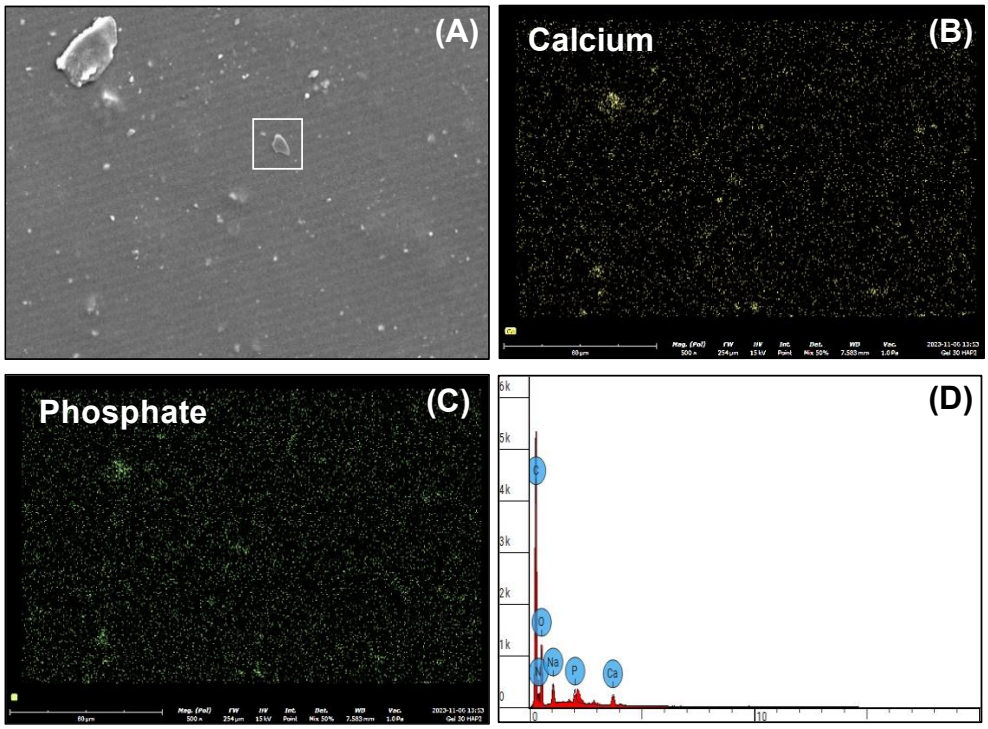

Figure 20 - Energy-dispersive X-ray spectroscopy mapping of GEL30-HAp2, including SEM image (A), Calcium element (B), Phosphate element (C) and EDXS spectrum of GEL30-HAp2 hydrogel (D).

Table 5 - Ca/P ratio present in GEL30-HAp2 hydrogel patches.

Material	Ca %w/w	P %w/w	Ca/P ratio
HAp	3.30	1.70	1.94

It was possible to identify the presence of calcium and phosphate, thus proving the presence of HAp in its constitution.

Figure 21 shows the SEM image and energy-dispersive X-ray spectroscopy mapping of GEL30-GO7.5-HAp2 hydrogel. Since this multimaterial hydrogel has GO, it is important to also qualify the presence of carbon and oxygen in its surface. This figure demonstrates the quantification of all the elements present in GEL30-GO7.5-HAp2 hydrogel, showed the same elements as GEL30-HAp2, as expected, since they were produced with the same components except for GO.

Figure 21A shows the SEM image of the hydrogel and Figure 21B, C, D, E and F, demonstrates the elements distribution: Carbon, calcium, phosphate, sodium, and oxygen, respectively.

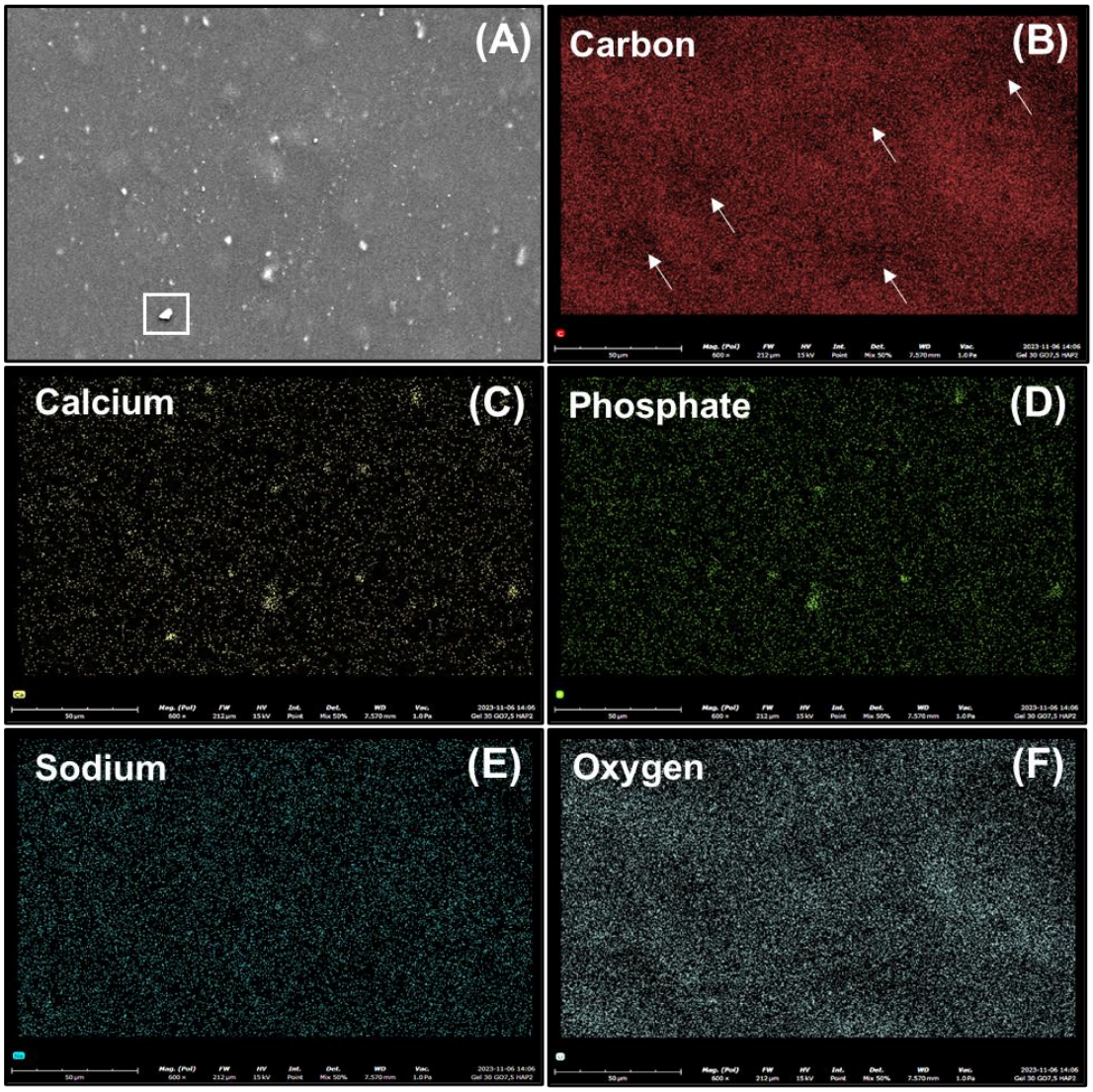

Figure 21 - Energy-dispersive X-ray spectroscopy mapping of GEL30-GO7.5-HAp2, including SEM image (A), Carbon element (B), Calcium element (C), Phosphate element (D), Sodium element (E) and Oxygen element (F).

Although GO is known to accelerate the reaction and this analysis is qualitative, the presence of carbon and oxygen is apparently consistently similar in all hydrogels (with or without GO). This demonstrates that the presence of other components does not impact element stability and distribution. The presence of GO is not noticeable because it is evenly distributed along the surface.

In GEL30-HAp2 and GEL30-GO7.5-HAp2 hydrogels, carbon, sodium, and oxygen elements are uniformly dispersed. The addition of NaOH to modify the pH causes the presence of sodium. However, it is demonstrated that its existence does not result in any other form of precipitation. Nevertheless, it is significant to observe the less concentrated spaces in the

carbon distribution. These spaces indicate the presence of HAp (calcium and phosphate) as shown through arrows in Figure 21B.

Table 6 demonstrates the Ca/P ratio in GEL30-GO7.5-HAp2 hydrogel. This makes it possible to prove the presence of HAp on the surface. Figure 22 demonstrates EDXS spectrum from a specific white cluster (indicated in Figure 21A), visually demonstrating the values shown in Table 6. Carbon is the element present in the most significant quantity in both multimaterial hydrogels.

Table 6 - Ca/P ratio present in GEL30-GO7.5-HAp2 hydrogel patches.

Material	Ca %w/w	P %w/w	Ca/P ratio
HAp	1.00	0.50	2.00

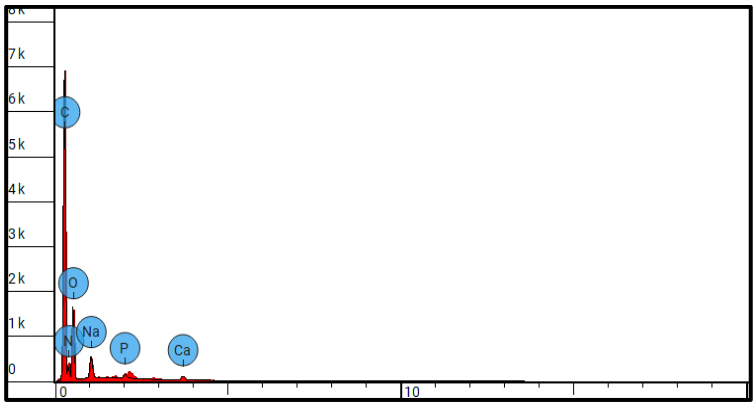

Figure 22 - EDXS spectrum of GEL30-GO7.5-HAp2 hydrogel.

4.3.2. Water Stability

Figure 23 depicts the water absorption capacity of each hydrogel, with variations based on its pre-test conditions. Figure 23A shows the results of the membranes at T0 (0 hours) and at the final time Tf (7 hours). Figure 23B demonstrates the graph with the behavior of the hydrogels based on equation 2, stored at 25ºC and 4ºC.

The experimental medium selected was water to facilitate a simple system free of interference from other ions and to assess if the medium was altered.

When dry hydrogels encounter water, water absorption by their matrix initiates and the weight increases. Water molecules initially bond directly to the hydrophilic groups, generating hydrophilically bound water. Consequently, the polymer network swells because of complete hydration of polar groups, exposing the hydrophobic groups [90]. The hydrogels stored at 4ºC exhibit visibly greater capacity to absorb water at room temperature than those stored at 25ºC.

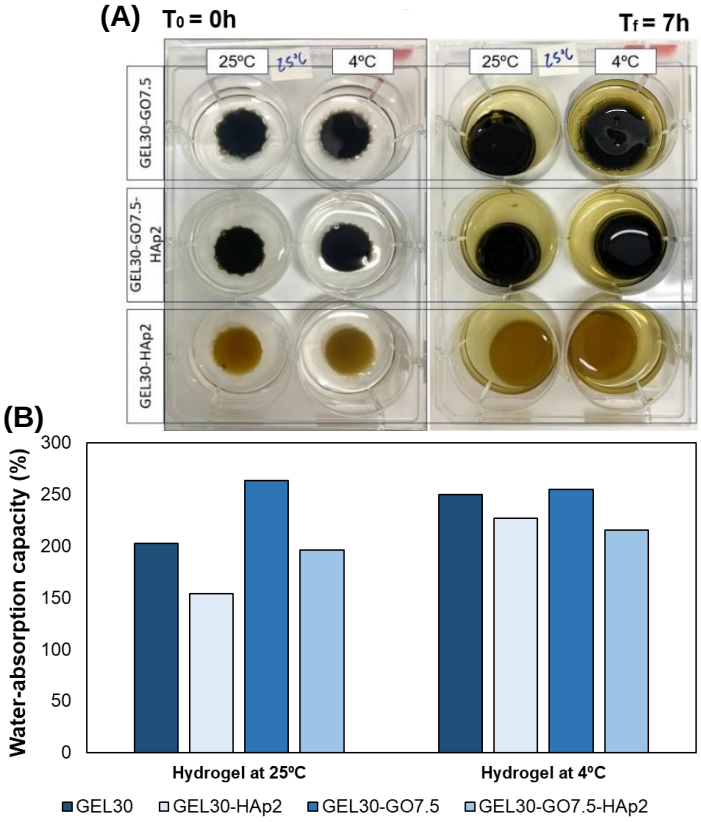

Figure 23 - Water-absorption capacity of the gelatin-based hydrogels stored at 25ºC and 4ºC. The assay was performed at 25ºC. (A) Visual results of the GEL30-GO7.5, GEL30-GO7.5-HAp2 and GEL30-HAp2 hydrogels at the initial (T0) and final times (Tf). (B) Graph displaying the behavior of the hydrogels based on equation 2.

The differences are evident for all the hydrogels except for GEL30-GO7.5, which was able to absorb more water at 25ºC, showing an increase in membrane diameter, i.e., an increase in volume. At the lower temperatures, it was observed that the composites swelled more when compared to the higher temperature [91].

It is also clear from Figure 23A that there is a loss of material present in the hydrogel to the medium. Based on its color, TA may be the suspected compound.

Based on Figure 23B, it can be inferred that the hydrogel with GO in its composition has a comparable water absorption capacity in both scenarios and consistently surpasses hydrogels lacking GO. This phenomenon can be justified by the structure of GO that confers unique interactions with water molecules, ultra-fast water transport mechanism, high hydrophilicity and expandable interlayer spacing. The formation of a hydrogen bond network with water micro-clusters in the confined GO laminates significantly affects the diffusion rate of water molecules and potential energy at the absorbed state. This, combined with GO's strong interaction with water, makes it a potential candidate for desiccant application [92].

The same assay was performed at 37ºC, to simulate the body temperature. The hydrogels were under the same conditions as above. Figure 24 shows the water absorption capacity of each hydrogel depending on their pre-test conditions. Figure 24A shows the results of the membranes at T0 (0 hours) and at the final time Tf (7 hours). Figure 24B demonstrates the graph with the behavior of the hydrogels based on equation 2, stored at 25ºC and 4ºC.

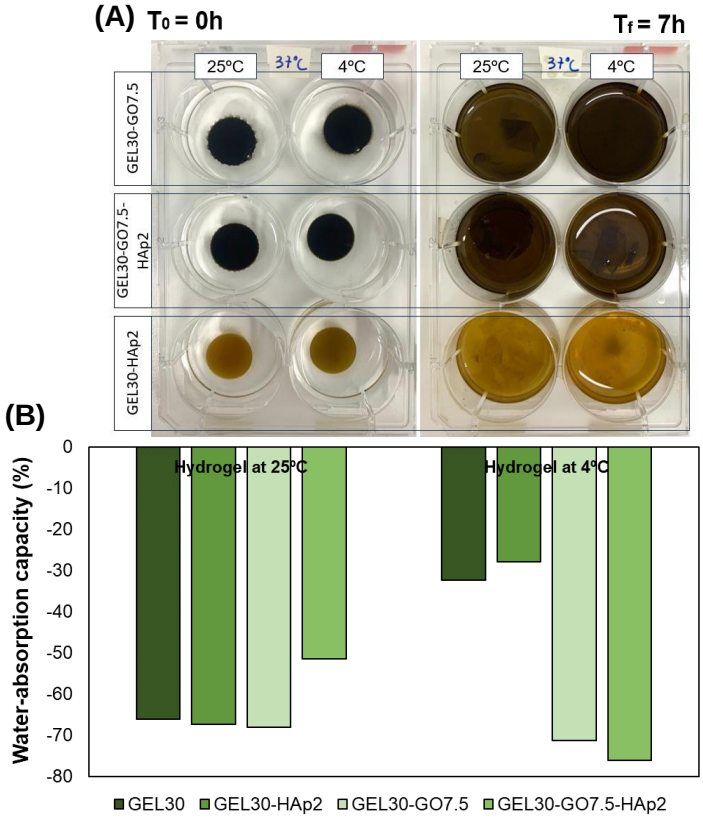

Figure 24 - Water-absorption capacity of the gelatin-based hydrogels stored at 25ºC and 4ºC. The assay was performed at 37ºC. (A) Visual results of the GEL30-GO7.5, GEL30-GO7.5-HAp2 and GEL30-HAp2 hydrogels at the initial (T0) and final times (Tf). (B) Graph displaying the behavior of the hydrogels based on equation 2.

Based on Figure 24, it is clearly seen that hydrogels that have been dried for only 1 day, whether stored at 25ºC or 4ºC, are unable to absorb water and cannot withstand a temperature of 37ºC in an aqueous environment.

Additionally, both hydrogels at 25ºC and 4ºC experienced a significant deterioration process that resulted in the complete loss of their structure, leaving only fragments of the film that was created by the presence of TA. The higher values for water absorption capacities of GEL30 and GEL30-HAp2 membranes at 4ºC are attributed to their inability to survive the entirety of the test, with complete degradation occurring at 60 and 120 minutes, respectively. In this assay, there is also a loss of material from the hydrogel in to the medium.

These hydrogels do not experience volume expansion in the presence of water at 37ºC and continually deteriorate as they lose volume. This experiment raised some important questions about the variables that could affect stability at 37ºC, such as the quantity of components added or the drying time of the hydrogel itself.

4.3.3. Degradation Ratio

The degradation ratio evaluation was performed on hydrogels with different post-production drying durations, limited to 21 days in 5 ml of PBS at 37ºC. The hydrogels were tested with drying durations of 1, 2, 7, and 15 days. The main objective of this investigation was to determine the required drying time for the hydrogels to maintain their structure at 37ºC in an aqueous environment.

The drying time of the hydrogel is a crucial parameter that impacts several properties, such as its internal structure; mechanical integrity, due to the formation of cross-links in the hydrogel structure, and if the drying time is not respected, it can lead to a fragile and less cohesive structure; and residual water content, if the hydrogel is not sufficiently dried, it can contain a percentage of residual water and can affect its stability and interactions with the surrounding environment [90]. This study highlights oxygen as a crucial component for the proper functioning and performance of hydrogels. When hydrogels with TA encounter oxygen, water is lost, and a thin insoluble film is formed, which only darkens the surface that is in contact with air due to the reaction with oxygen.

Figure 25 exhibits the formation of an insoluble and resistant film on the surface of the hydrogel control that was exposed to oxygen after one day, illustrating this phenomenon. This process affects the mechanical strength and rigidity of the material. As a cross-linking agent, TA creates chemical bonds between polymer chains, forming a 3D structure in the polymer matrix. This results in a more rigid and stable material with improved mechanical properties [42, 94].

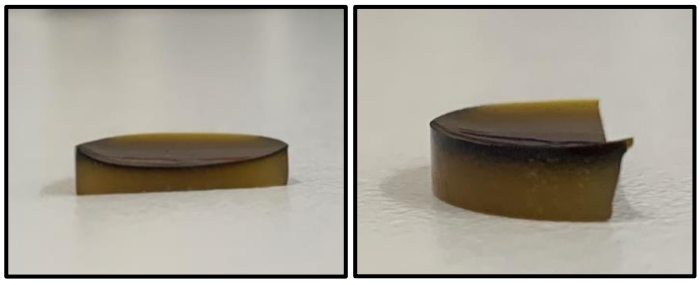

Figure 25 - A film formed on the exposed surface of the hydrogel control after one day of oxygen exposure.

Figure 26 shows the degradation ratio of the gelatin-based hydrogels dried for 15 days. Figure 26A illustrates the visual differences between the test at time 0 and after 21 days. Most of the hydrogels were visibly degraded, except for those containing HAp-NPs, which maintained their form until the end of the test, despite a lower weight compared to the initial weight. It can be inferred that there was a loss of hydrogels' material in the PBS medium. Figure 26B demonstrates the behavior of the hydrogels based on equation 3.

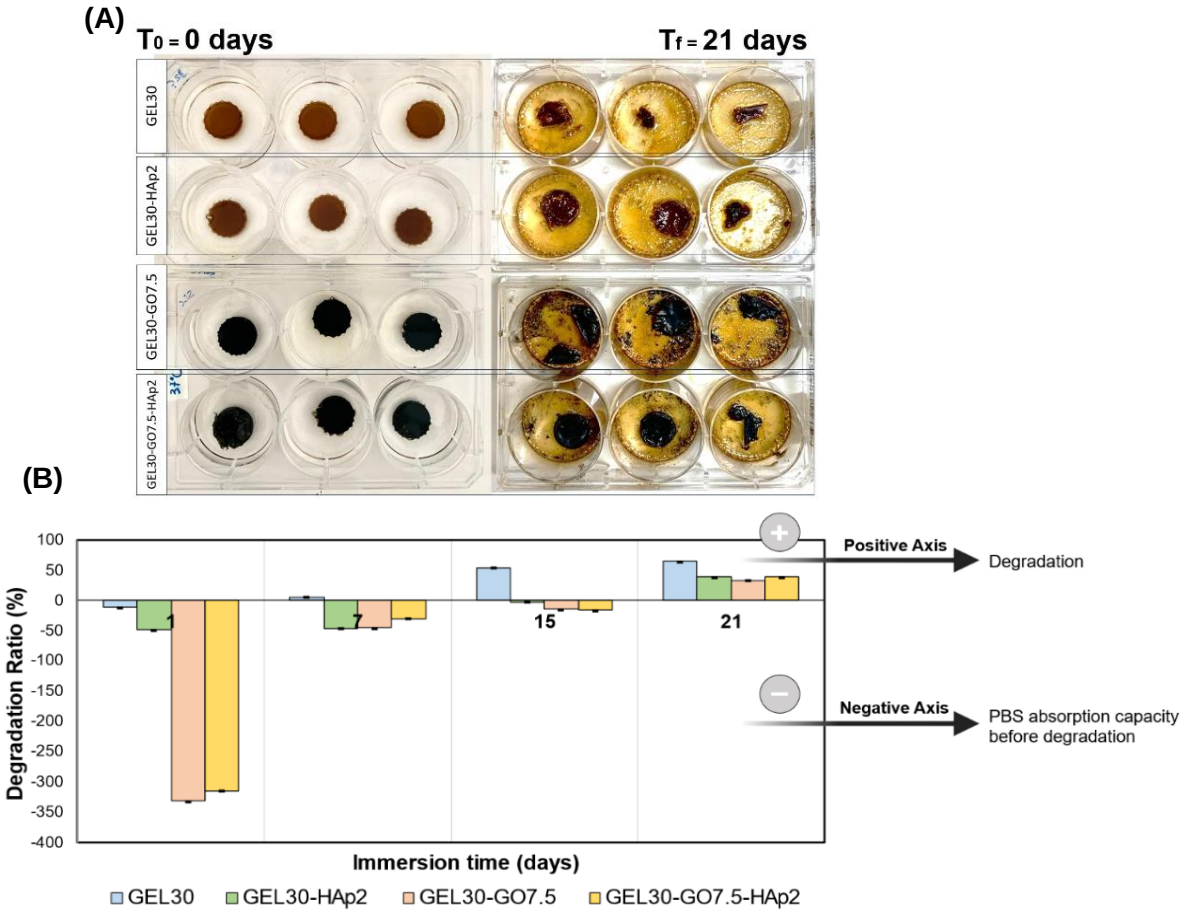

Figure 26 - Degradation ratio (%) of the gelatin-based hydrogels dried for 15 days. These hydrogels were tested for 21 days in PBS solution. (A) Visual results of the GEL30, GEL30-GO7.5, GEL30-GO7.5-HAp2 and GEL30-HAp2 hydrogels at the initial (T0) and final times (Tf), after 21 days. (B) Graph displaying the behavior of the hydrogels based on equation 3.

The degradation ratio was calculated for all hydrogels with varying drying times (data not shown) using equation 3. It was verified that only the hydrogels dried for 15 days were able to withstand the 21-day period. It is important to mention that the longer the drying time was, the less flexible the hydrogel became [94].

Analyzing the plot, it is important to note that if the values are negative, they indicate that the hydrogels have not suffered degradation, but rather an increase in volume due to the

absorption of the solution; if the values are positive, degradation occurs, and their structures are no longer uniform. It can be observed that all hydrogels experienced degradation after undergoing 21 days of immersion, regardless of their compositions.

The hydrogels GEL30-HAp2, GEL30-GO7.5, and GEL30-GO7.5-HAp2 effectively absorbed PBS for 15 days without experiencing any volume loss, unlike GEL30 which rapidly lost its water-retaining ability on day 1. While GEL30 exhibited a faster degradation rate, the remaining hydrogels initiated degradation only after 21 days.

The hydrogels containing GO and HAp-NPs showed, as expected, better results in terms of maintaining their structure up to 21 days. The presence of GO results in increased rigidity and stability of the hydrogels at 37ºC. On the other hand, HAp-NPs increase the hydrogel's network, enabling it to absorb more solution and increase its volume. The hydrogels containing GO and GO mixed with Hap exhibited superior performance by displaying stability and degradation resistance for up to 21 days at 37ºC in PBS.

4.3.4. Mechanical Properties

Tensile tests were conducted to investigate the effect of GO and HAp on the mechanical properties of gelatin-based hydrogels. Figure 27 displays the test specimens, including their initial state after production (Figure 27A). The beginning of the test is also shown in Figure 27B and the point of fracture (Figure 27C). The demonstration curves Stress-Distance for each individual specimen tested are present in Figure 27D.

The Stress-Distance curves reveal that the GEL30-GO7.5 hydrogel exhibited a higher stress with an ultimate strength of approximately 678KPa compared to the GEL30-HAp2 hydrogel which only reached a value of 438KPa. The disparity can be attributed to the presence of GO and HAp-NPs. GO provides greater resistance to the hydrogel owing to its inherent mechanical properties, whereas HAp-NPs provide greater elasticity to the hydrogel in exchange for greater resistance to stress. When the GEL30-GO7.5-HAp2 curve is examined, it is evident that the combination of these two components results in a relatively high ultimate strength compared to that of the control (GEL30) and is very similar to the hydrogel that only contains GO, which exhibits an ultimate strength of approximately 610KPa. The hydrogel acquires superior resistance characteristics after the GO and HAp-NPs are combined but its structure becomes more elastic as it contains HAp-NPs.

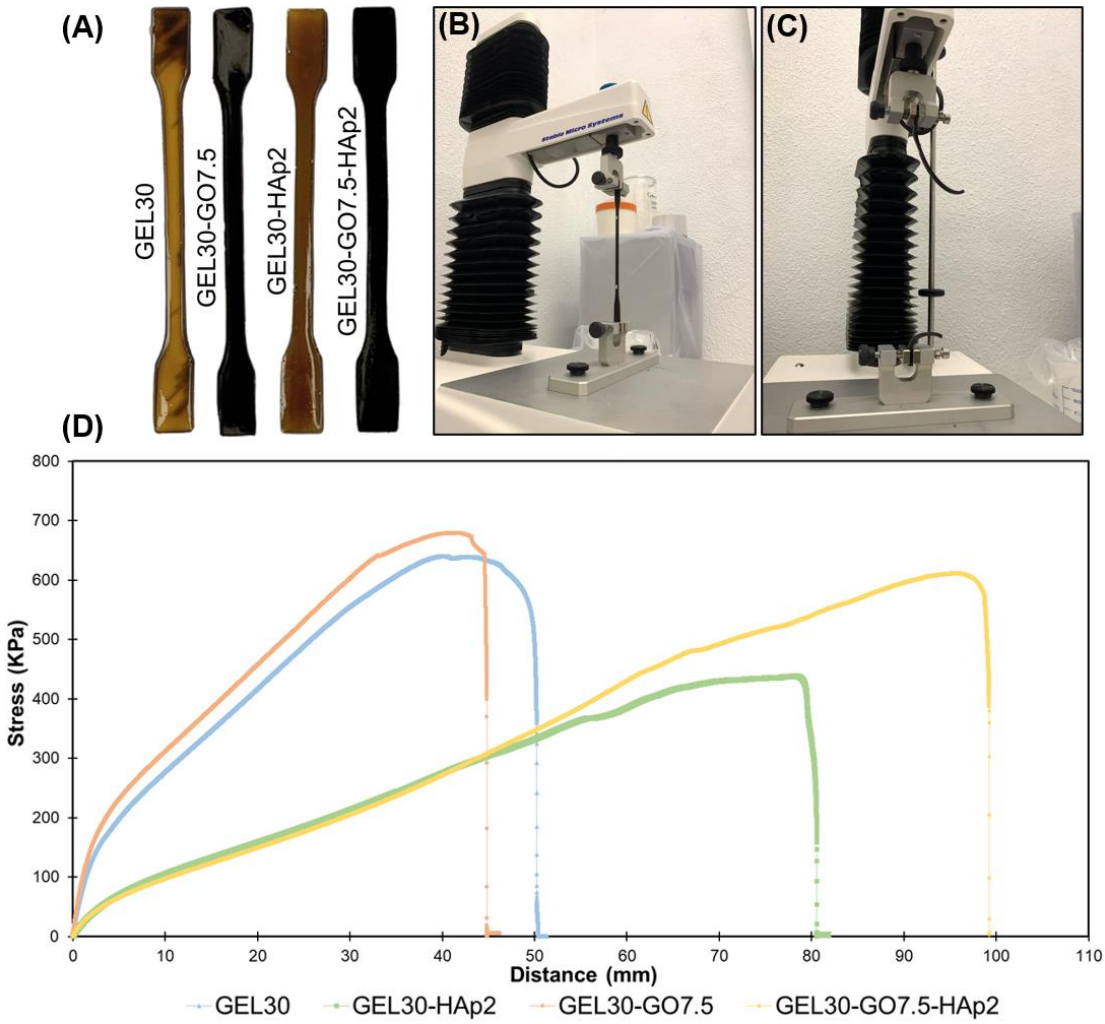

Figure 27 - Tensile testing. (A) Hydrogel specimens after their production. (B-C) The tensile test before and after fracture, respectively. (D) Stress-Distance curves are representative of all the hydrogels.

The addition of GO in this study aimed to enhance their mechanical properties [95]. Therefore, this test confirms that GO provides these desirable features to the hydrogels, resulting in increased rigidity of the hydrogels.

A study by Lee *et. al* [96] analyzed that by increasing the percentage of GO present in a structure printed with HAp, the modulus of elasticity decreases [96]. In this case – Figure 27D – It is not possible to calculate the Young's Modulus. However, in the presence of HAp, the modulus value would be expected to decrease when GO is included in the hydrogel (GEL30-GO7.5-HAp2) compared to when the hydrogel has only GO in its composition (GEL30-GO7.5).

Gaharwar and his collaborators [91] investigated the effect of various percentages of HAp-NPs on the mechanical properties of a composite with poly(ethylene glycol) and showed that, as the percentage of HAp increases, the modulus of elasticity also increases [91]. Based on their study, it is anticipated that hydrogels containing 2% HAp-NPs will exhibit greater fracture strength and increased tensile modulus compared to the control hydrogels [91].

It is possible to conclude that the hydrogel containing both HAp-NPs and GO demonstrates an increase in resistance and elasticity to the hydrogels, revealing that the mechanical properties are affected by their presence.

4.4. 3D Printing Process

The 3D printing process requires specific characteristics for optimal functioning. As discussed earlier, it is essential to optimize the printing speed, pressure, and temperature to achieve the highest precision possible.

4.4.1. Strand and line tests

Temperature plays a crucial role in the printing process and the required formulations were identified through prior rheological studies to determine the optimal conditions for efficient extrusion. To optimize filament temperature, a series of strand tests were conducted until the proper gelation was achieved. Figure 28 shows the three types of gelation occurred in the nozzle during extrusion until the ideal temperature was reached for the specific nozzle type.

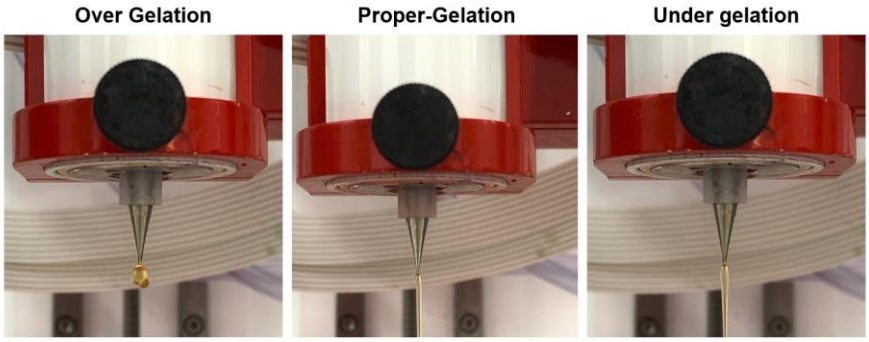

Figure 28 - Strand tests. Different temperatures result in different types of gelation.

Over gelation occurs when the temperature is below the gelation point, and under gelation occurs when the temperature is well above the gelation point, which is characterized by low viscosity. The proper-gelation is the right temperature for printing. The prior conducted rheological tests were critical in determining the appropriate gelling temperature. These tests provided information on the gelation temperature, which allows the optimal gelation temperature to be assumed to be always higher than the crossover temperature (G'=G''). The appropriate temperature can vary depending on the type of nozzle used; nevertheless, the fundamental principle must remain consistent.

The line test is a crucial evaluation performed prior to the final printing process. It is fundamental in the process of selecting the correct and appropriate velocity for the print and

allows the analysis of three different types (10mm/s, 20mm/s and 30mm/s). The analysis enables the user to compare the nozzle used with the prints obtained, to determine which velocity has the highest precision. This evaluation measures the width and length of printed lines to determine which setting provides the greatest accuracy.

The Length Index was used to assess print accuracy [31]. Kang *et al.* [97] determined, based on quantitative image analysis, the print accuracy and resolution along the length, width and height. The principle used was quantifying the print outcome though printing samples dimensioned. They developed a method to achieve Length Index that compares the theoretical print to the effective print that allows to categorize the offset in length between the designed and the printed path [97], demonstrated in equation 4. This index ranged from 0 to 1, where index of 1 indicated perfect match with no underprinted and overprinted length. In addition, Kang and his collaborators [97] also investigated the print resolution by defining a dimensionless variable Width Index to analyze results through the width. The Width Index was achieved by comparing the average width of the printed path and the nozzle diameter, as demonstrated in equation 5.

For the Length Index (equation 4), only one point is measured on each line. For the width measurement (equation 5), three points are measured on each line and the average is divided by the nozzle diameter. Once the measurements are complete, index results with values equal to or near 1 determine the correct velocity.

Figure 29 shows the line test for GEL30-GO7.5-HAp2 and the respective Length and Width Index.

Lenght Index measurements

	10mm/s	Lenght Index (mm)	20mm/s	Lenght Index (mm)	30mm/s	Lenght Index (mm)
	36.212	0.905	38.572	0.9643	38.994	0.975
	38.992	0.975	38.573	0.964	39.910	0.998
	39.327	0.983	37.728	0.943	39.414	0.985
Mean	38.177	0.954	38.291	0.957	39.439	0.986
Standard Deviation	1.710	0.043	0.488	0.012	0.459	0.011

Width Index measurements

	10mm/s	Width Index (mm)	20mm/s	Width Index (mm)	30mm/s	Width Index (mm)
	1.266	2.897	0.758	1.735	0.465	1.064
	1.095	2.506	1.014	2.320	0.549	1.256
	0.842	1.927	1.014	2.320	0.505	1.156
	1.263	2.890	0.674	1.542	0.463	1.059
	1.432	3.277	0.758	1.735	0.589	1.348
	1.274	2.915	0.763	1.746	0.379	0.867
	1.098	2.513	0.595	1.362	0.505	1.156
	1.011	2.314	0.758	1.735	0.547	1.252
	1.095	2.506	0.589	1.348	0.505	1.156
Mean	1.153	2.638	0.769	1.760	0.501	1.146
Standard Deviation	0.175	0.400	0.155	0.355	0.061	0.140

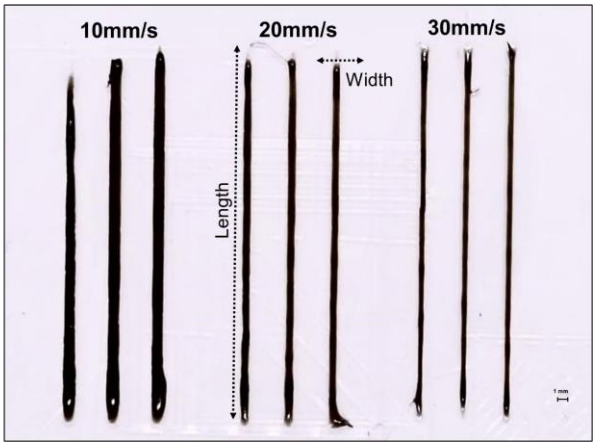

Figure 29 - Line test. Printed filaments to obtain length and width index measurements.

The study demonstrates that the optimal speed for this formulation type, using the 25G white nozzle, is 30mm/s. This speed resulted in a Length Index of 0.986mm and a Width Index of 1.146mm.

4.4.2. 3D Printed Constructs

All the multimaterial formulations were printed with three layers with the same angles orientation with the parameters enumerated in Table 3. The formulations with HAp-NPs were printed as gum patches and the others as squares, in order to distinguish and diversify the geometry. Figure 30 shows all the printed structures.

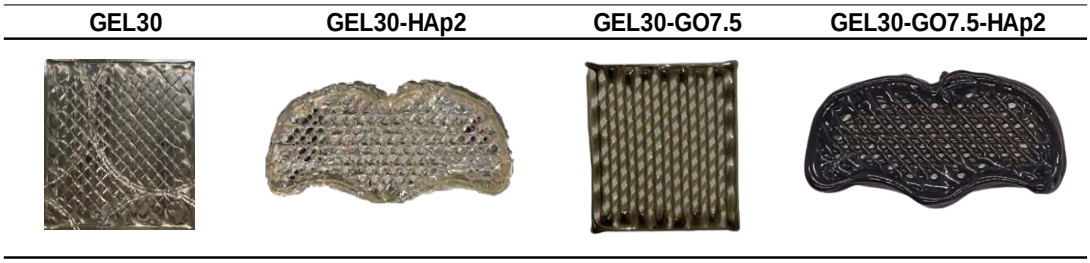

Figure 30 - 3D printed constructs of all the formulations in two different geometries.

It can be concluded that GEL30, GEL30-HAp2, GEL30-GO7.5 and GEL30-GO7.5-HAp2 were effectively printed, and their porosity is evident in all hydrogels, as can be seen in Figure 30. Incorporating nanoparticles and GO into the gelatin base did not impact printing accuracy. All multimaterial formulations can be printed by adjusting the parameters according to previously studied rheological properties. This was confirmed by the line test on the GO and HAp mixture formulation, displaying expected precision under these conditions.

A composite hydrogel system is a valuable method for incorporating and blending diverse hydrogel functions and characteristics that cannot be accomplished with a single hydrogel. By utilizing 3D printing, it is achievable to develop a structure with increased capabilities [98].

Wüst *et al.* [99] incorporated HAp-NPs into a hydrogel system consisting of gelatin and alginate for the purpose of enhancing the printability and mechanical stability of bone tissue engineering. Gelatin, whose crosslinking behavior is temperature-dependent, provided initial viscosity and stability for 3D printing, while the ionic crosslinking of alginate achieved long-term stability. Using a heatable cartridge-equipped 3D-bioplotter, the team successfully printed structures with superior printability at 40°C. The incorporation of 8% w/v HAp nanoparticles resulted in a substantial increase in Young's modulus over a three-day incubation span. They concluded that the inclusion of HAp also favors the use of bioink for bone tissue engineering applications.

Li and his collaborators [100] developed a 3D printable GO based bio-ink for cell support and tissue engineering. Rheology studies demonstrated that adding GO [0.1% or 0.5% (w/w)], provided higher storage modulus than loss modulus to the dispersion, indicating that the addition of GO up to 0.5% (w/w) does not influence printability. The scaffolds were printed with

different GO concentrations and with multi-angle design. The results showed that 0.05% (w/w) and 0.1% (w/w) GO content inks exhibited improved resolution due to improved storage modulus to retain strut structure after extrusion and flowability during extrusion. It was concluded that the incorporation of 0.05%–0.1% (w/w) GO in an Alginate/Gel hydrogel improves 3D printability of the gel, including printing resolution. The addition of GO also proved to improve cell-affinity of bioinert biomaterials by providing more bioactive moieties on the scaffold surface.

4.4.2.1. Porosity measurements

Porosity is crucial in the treatment of periodontitis by facilitating the diffusion of nutrients and oxygen, as well as cell infiltration, promoting cell growth and new tissue formation; preventing bacterial invasion, promoting a sterilized environment for regeneration without infectious complications; and, most importantly, tissue accommodation itself, which allows the hydrogel to adapt to the periodontal space, providing physical and structural support for tissue growth [101, 102]. Porosity was achieved by producing three layers of hydrogel at different angles, which was confirmed by microscopic images by GEL30-HAp2 and GEL30-GO7.5-HAp2 (Figure 31). The porosity is visible to the naked eye, but a more precise analysis of the different layers can be achieved with the aid of either a magnifying glass or a microscope.

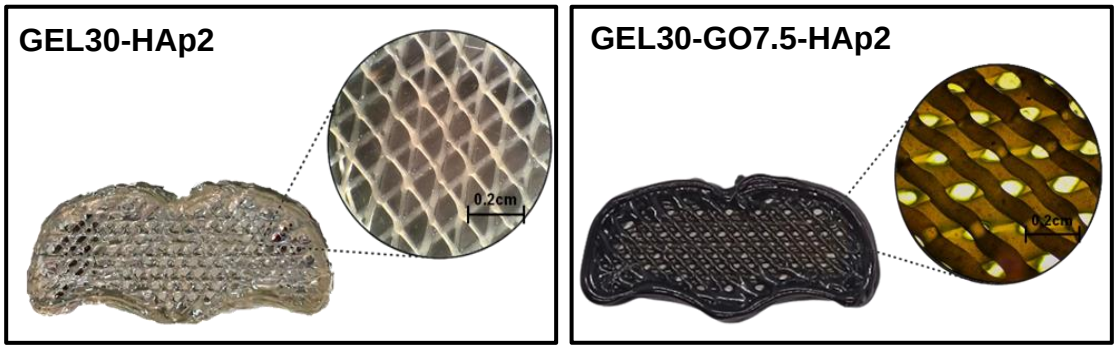

Figure 31 - GEL30-HAp2 and GEL30-GO7.5-HAp2 gum patches with 30x and 100x magnification, respectively.

At a magnification of 400x, Figure 32 exhibits the diverse layers of GEL30-GO7.5-HAp2 containing all the compounds. This microscopic view shows different clusters of nanoparticles that may belong to HAp-NPs or GO. This analysis does not enable the precise identification of which elements are present in the clusters. A few particles derived from the GO suspension are also visible, as can be seen by the circles in Figure 32.

The area of the pores identified through black arrows was calculated using ImageJ. The values for the area of each pore are shown in Figure 32 and Table 7.

Although the images are to scale, the pores may not be fully visible, so these values can only be considered characteristic of what is observed in the figure.

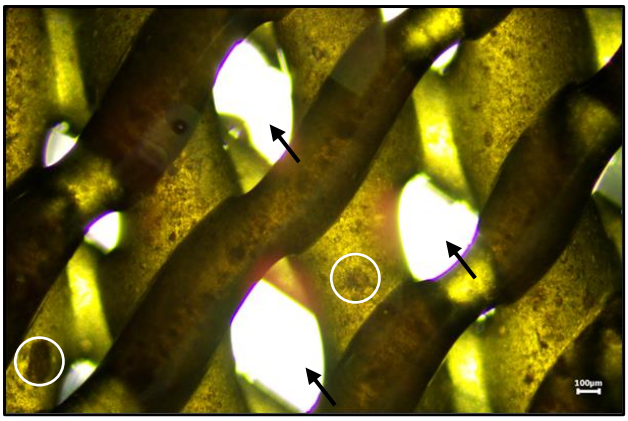

Figure 32 - Porosity of GEL30-GO7.5-HAp2 at 400x magnification.

Table 7 - Area average and standard deviation of the pores presented in Figure 32.

	Pore 1	Pore 2	Pore 3	Mean	Standard Deviation
Area (mm^2)	118.71	101.04	157.52	125.76	28.89

After evaluating the different hydrogels, it can be inferred that the hydrogel with the most advantageous characteristics and the most beneficial properties for the purpose of the study is GEL30-GO7.5-HAp2. This hydrogel contains study-proven components with both anti-microbial and osteoinductive properties: HAp and GO. These characteristics establish it as an exceptional candidate for application in periodontal diseases. Not only is it the most complete hydrogel in terms of its composition, but it also showed a good degradation rate (up to 21 days in PBS) and its mechanical properties offered good resistance to stress and elasticity, which may be beneficial given the area where it will be applied. To determine whether the study was successful, 3D printing proved that it is possible to print this hydrogel effectively, accurately, and reproducibly.

Chapter 5 - Conclusion and Future Work

5.1. Conclusion

The results of this study demonstrated that it is possible to develop gelatin-based multimaterial membranes functionalized with nanoparticles with antibacterial, anti-inflammatory and osteoinductive properties using 3D printing.

The HAp synthesis process proved to be successful, producing nanoparticles with the expected nanorod shape.

The rheological analysis showed that the balance between the viscous and elastic moduli was crucial for achieving stable and precise 3D printed structures. Furthermore, the addition of GO significantly increased the elastic behavior of the formulations. However, excessive quantities of GO (37.5%) were found to be detrimental to 3D printing, leading to an adjustment of the formulations by reducing GO content, increasing HAp, and the addition of glycerin. The optimized multimaterial formulations exhibited similar rheological behavior and gelling temperatures. The viscosity values increased at lower temperatures, which is critical for stable 3D printing.

The ATR-FTIR analysis enabled the identification of different bands present in the hydrogel to understand the effect of HAp on its composition, identifying characteristic bands of gelatin, PVA, TA, and GO.

SEM images confirmed uniform distributions of GO and HAp, while EDS analysis established the existence of HAp in the hydrogel compositions.

Water stability tests revealed that water absorption capacities were temperature-dependent, with GO-containing hydrogels demonstrating superior performance attributed to their specific interactions with water molecules. Degradation studies highlighted the significance of drying time, showing that hydrogels containing GO and HAp with 15 days of drying possessed stability over 21 days.

Moreover, tensile tests demonstrated that GO enhanced hydrogel strength and improved the mechanical properties. The integration of GO and HAp resulted in well-balanced mechanical performance. The 3D printing process achieved success, with optimized speeds identified through strand and line tests. Porosity measurements have shown that it is possible to fabricate porous structures with controlled pore sizes through different angles.

In conclusion, the main goals of this work were achieved. The final formulation chosen (GEL30-GO7.5-HAp2) allowed the development of gelatin-based multimaterial hydrogels, exhibiting promising rheological properties, structural stability, mechanical strength, and 3D printing capabilities with great printability and reproducible results. The incorporation of GO and HAp presents a flexible platform for biomedical uses such as tissue engineering, with precise control over material properties and structure being imperative in such application. Further research could investigate targeted applications and customize formulations for specific functionalities, particularly in the context of the different stages of periodontal disease.

5.2. Future work

Although the main goals of the proposed work have been achieved, there is always room for improvement.

An important aspect for hydrogels is their ability to absorb water, swell and withstand degradation. Finding an alternative method to accelerate drying of the hydrogels would improve their overall performance. To obtain a more thorough comprehension of the water absorption capacity, it is vital to conduct a detailed examination of the expansion ratio and water content in the 3D constructs developed. Additionally, the same procedures should be performed on the 3D printed structures, to determine if their structure is modified.

Another valuable approach would be to further study the interaction of these hydrogels with cells and biological tissues. Gaining a better comprehension of the mechanisms by which these materials interact within the biological environment could offer important insights for clinical and therapeutic purposes. It is crucial to conduct extended testing of these hydrogels *in vivo*.

References

[1] “Periodontitis - Diagnosis and treatment - Mayo Clinic,” 2023. https://www.mayoclinic.org/diseases-conditions/periodontitis/diagnosis-treatment/drc-20354479 (accessed Aug. 21, 2023).

[2] L. M. Sedghi, M. Bacino, and Y. L. Kapila, “Periodontal Disease: The Good, The Bad, and The Unknown,” *Front. Cell. Infect. Microbiol.*, vol. 11, Dec. 2021, doi: 10.3389/FCIMB.2021.766944.

[3] S. Torabi and A. Soni, “Histology, Periodontium,” *StatPearls*, Mar. 2023, Accessed: Nov. 10, 2023. [Online]. Available: https://www.ncbi.nlm.nih.gov/books/NBK570604/.

[4] B. A. Niemiec, “Periodontal Disease,” *Top. Companion Anim. Med.*, vol. 23, no. 2, pp. 72–80, 2008, doi: 10.1053/j.tcam.2008.02.003.

[5] J. L. Muñoz-Carrillo *et al.*, “Pathogenesis of Periodontal Disease,” *Periodontal Dis. - Diagnostic Adjunctive Non-surgical Considerations*, Jun. 2019, doi: 10.5772/INTECHOPEN.86548.

[6] H. B. Lobprise and J. Johnson, “Periodontal Disease,” *Pet-Specific Care Vet. Team*, pp. 271–275, Apr. 2023, doi: 10.1002/9781119540687.ch4.

[7] G. Hajishengallis, “Interconnection of periodontal disease and comorbidities: Evidence, mechanisms, and implications,” *Periodontol. 2000*, vol. 89, no. 1, pp. 9–18, 2022, doi: 10.1111/prd.12430.

[8] Y. N. Chen, L. Peng, T. Liu, Y. Wang, S. Shi, and H. Wang, “Poly(vinyl alcohol)-Tannic Acid Hydrogels with Excellent Mechanical Properties and Shape Memory Behaviors,” *ACS Appl. Mater. Interfaces*, vol. 8, no. 40, pp. 27199–27206, Oct. 2016, doi: https://doi.org/10.1021/acsami.6b08374.

[9] D. C. LYONS, “The Healthy Mouth,” *AJN, Am. J. Nurs.*, vol. 31, no. 10, pp. 1169–1172, 1931, doi: 10.1097/00000446-193110000-00011.

[10] A. Palumbo, “The Anatomy and Physiology of the Healthy Periodontium, Gingival Diseases - Their Aetiology, Prevention and Treatment,” 2011. doi: 10.5772/25275.

[11] M. Katafuchi, T. Matsuura, P. Atsawasuwan, H. Sato, and M. Yamauchi, “Biochemical Characterization of Collagen in Alveolar Mucosa and Attached Gingiva of Pig,” *Connect. Tissue Res.*, vol. 48, no. 2, pp. 85–92, Mar. 2007, doi: 10.1080/03008200601143508.

[12] H. Chen and Y. Liu, *Teeth*. Elsevier Inc., 2014.

[13] P. D. Laird C Sheldahl, “Histology of tooth and periodontal tissues,” in *Histology and Embryology for Dental Hygiene*, 2020.

[14] R. G. Fischer *et al.*, “Periodontal disease and its impact on general health in Latin America. Section V: Treatment of periodontitis,” *Braz. Oral Res.*, vol. 34, pp. 1–9, 2020, doi: 10.1590/1807-3107BOR-2020.VOL34.0026.

[15] “Periodontitis (Gum Disease): Symptoms, Stages & Treatment.” https://my.clevelandclinic.org/health/diseases/16620-periodontitis (accessed Nov. 13, 2023).

[16] M. Zieba *et al.*, “Polymeric carriers for delivery systems in the treatment of chronic periodontal disease,” *Polymers (Basel).*, vol. 12, no. 7, pp. 1–21, 2020, doi: 10.3390/polym12071574.

[17] E. Nishida *et al.*, “Graphene oxide scaffold accelerates cellular proliferative response and alveolar bone healing of tooth extraction socket,” *Int. J. Nanomedicine*, vol. 11, pp. 2265–2277, May 2016, doi: 10.2147/IJN.S104778.

[18] M. Z. I. Nizami, I. X. Yin, C. Y. K. Lung, J. Y. Niu, M. L. Mei, and C. H. Chu, “In Vitro Studies of Graphene for Management of Dental Caries and Periodontal Disease: A Concise Review,” *Pharmaceutics*, vol. 14, no. 10, Oct. 2022, doi: 10.3390/PHARMACEUTICS14101997.

[19] M. P. Mani *et al.*, “A review on 3D printing in tissue engineering applications,” *J. Polym. Eng.*, vol. 42, no. 3, pp. 243–265, Mar. 2022, doi: https://doi.org/10.1515/polyeng-2021-0059.

[20] S. H. Kim *et al.*, “4D-bioprinted silk hydrogels for tissue engineering,” *Biomaterials*, vol. 260, no. August, 2020, doi: 10.1016/j.biomaterials.2020.120281.

[21] S. Knowlton, S. Anand, T. Shah, and S. Tasoglu, “Bioprinting for Neural Tissue Engineering,” *Trends Neurosci.*, vol. 41, no. 1, pp. 31–46, Jan. 2018, doi: 10.1016/J.TINS.2017.11.001.

[22] T. Jiang, J. G. Munguia-Lopez, S. Flores-Torres, J. Kort-Mascort, and J. M. Kinsella, “Extrusion bioprinting of soft materials: An emerging technique for biological model fabrication,” *Appl. Phys. Rev.*, vol. 6, no. 1, Mar. 2019, doi: 10.1063/1.5059393.

[23] C. Mandrycky, Z. Wang, K. Kim, and D. H. Kim, “3D bioprinting for engineering complex tissues,” *Biotechnol. Adv.*, vol. 34, no. 4, pp. 422–434, Jul. 2016, doi: 10.1016/J.BIOTECHADV.2015.12.011.

[24] H. J. Lee, Y. W. Koo, M. Yeo, S. H. Kim, and G. H. Kim, “Recent cell printing systems for tissue engineering,” *Int. J. Bioprinting*, vol. 3, no. 1, pp. 27–41, 2017, doi: 10.18063/IJB.2017.01.004.

[25] F. Sivandzade and L. Cucullo, “In-vitro blood–brain barrier modeling: A review of modern and fast-advancing technologies,” *J. Cereb. Blood Flow Metab.*, vol. 38, no. 10, pp. 1667–1681, 2018, doi: 10.1177/0271678X18788769.

[26] N. Li, R. Guo, and Z. J. Zhang, “Bioink Formulations for Bone Tissue Regeneration,” *Front. Bioeng. Biotechnol.*, vol. 9, no. February, pp. 1–17, 2021, doi: 10.3389/fbioe.2021.630488.

[27] M. Soori, “Applications of Additive Manufacturing to Tissue Engineering,” 2019. [Online]. Available: https://www.researchgate.net/publication/332570568_Applications_of_Additive_Manufacturing_to_Tissue_Engineering.

[28] S. Rahmani, A. Olad, and Z. Rahmani, “Preparation of self-healable nanocomposite hydrogel based on Gum Arabic/gelatin and graphene oxide: study of drug delivery behavior,” *Polym. Bull.*, vol. 80, no. 4, pp. 4117–4138, 2023, doi: 10.1007/s00289-022-04247-6.

[29] H. Herrada-Manchón, M. A. Fernández, and E. Aguilar, “Essential Guide to Hydrogel Rheology in Extrusion 3D Printing: How to Measure It and Why It Matters?,” *Gels*, vol. 9, no. 7, 2023, doi: 10.3390/gels9070517.

[30] H. Li, “Study of hydrogels for 3D printing of constructs with strong interfacial bonding,” Nanyang Technological University, Singapore, 2018.

[31] S. Bom, R. Ribeiro, H. M. Ribeiro, C. Santos, and J. Marto, “On the progress of hydrogel-based 3D printing: Correlating rheological properties with printing behaviour,” *Int. J. Pharm.*, vol. 615, pp. 1–14, 2022, doi: 10.1016/j.ijpharm.2022.121506.

[32] J. Ahmed, *Rheological Properties of Gelatin and Advances in Measurement*. Elsevier Ltd, 2017.

[33] S. Bashir *et al.*, “Fundamental Concepts of Hydrogels: Synthesis, Properties, and Their Applications,” *Polymers (Basel).*, vol. 12, no. 2702, pp. 1–60, 2020, doi: 10.3390/polym12112702.

[34] Y. S. Zhang and A. Khademhosseini, “Advances in engineering hydrogels,” *Science*, vol. 356, no. 6337, pp. 1–27, May 2017, doi: 10.1126/SCIENCE.AAF3627.

[35] X. Wang *et al.*, “Gelatin-based hydrogels for organ 3D bioprinting,” *Polymers (Basel).*, vol. 9, no. 9, 2017, doi: 10.3390/polym9090401.

[36] S. Chauhan *et al.*, *Development, optimization and evaluation of curcumin loaded biodegradable crosslinked gelatin film for the effective treatment of periodontitis*, vol. 44, no. 7. Taylor & Francis, 2018.

[37] I. J. Haug and K. I. Draget, “Gelatin,” *Handb. Food Proteins*, pp. 92–115, Jan. 2011, doi: 10.1533/9780857093639.92.

[38] T. U. Rashid *et al.*, “Gelatin-Based Hydrogels,” in *Cellulose-Based Superabsorbent Hydrogels*, 2019, pp. 1601–1641.

[39] C. Li, L. Zhao, J. Han, R. Wang, C. Xiong, and X. Xie, “Synthesis of citrate-stabilized hydrocolloids of hydroxyapatite through a novel two-stage method: a possible aggregates-breakdown mechanism of colloid formation,” *J. Colloid Interface Sci.*, vol. 360, no. 2, pp. 341–349, Aug. 2011, doi: 10.1016/J.JCIS.2011.04.059.

[40] D. Huang, Z. Zhang, Q. Quan, and Y. Zheng, “Tannic acid: A versatile and effective modifier for gelatin/zein composite films,” *Food Packag. Shelf Life*, vol. 23, p. 100440, Mar. 2020, doi: 10.1016/J.FPSL.2019.100440.

[41] H. Jafari *et al.*, “Tannic acid: a versatile polyphenol for design of biomedical hydrogels,” *J. Mater. Chem. B*, vol. 10, no. 31, pp. 5873–5912, Aug. 2022, doi: 10.1039/D2TB01056A.

[42] X. Zhang *et al.*, “Chemical modification of gelatin by a natural phenolic cross-linker, tannic acid,” *J. Agric. Food Chem.*, vol. 58, no. 11, pp. 6809–6815, 2010, doi: 10.1021/jf1004226.

[43] M. K. Arumugam, M. C. Paal, T. M. Donohue, M. Ganesan, N. A. Osna, and K. K. Kharbanda, “Beneficial Effects of Betaine: A Comprehensive Review,” *Biology (Basel).*, vol. 10, no. 6, p. 456, May 2021, doi: 10.3390/BIOLOGY10060456.

[44] G. Zhao *et al.*, “Betaine in Inflammation: Mechanistic Aspects and Applications,” *Front. Immunol.*, vol. 9, no. MAY, p. 1070, May 2018, doi: 10.3389/FIMMU.2018.01070.

[45] A. Rodríguez-Agurto *et al.*, “Randomized clinical trial on the clinical effects of a toothpaste containing extra virgin olive oil, xylitol, and betaine in gingivitis,” *Sci. Rep.*, vol. 13, no. 1, pp. 1–8, 2023, doi: 10.1038/s41598-023-33521-4.

[46] C. C. Demerlis and D. R. Schoneker, “Review of the oral toxicity of polyvinyl alcohol (PVA),” *Food Chem. Toxicol.*, vol. 41, no. 3, pp. 319–326, 2003, [Online]. Available: https://kundoc.com/pdf-review-of-the-oral-toxicity-of-polyvinyl-alcohol-pva-.html.

[47] T. Regeneration, “3D-Printed Soft Membrane for Periodontal Guided,” 2023.

[48] H. Y. Jeong *et al.*, “Graphene oxide thin films for flexible nonvolatile memory applications,” *Nano Lett.*, vol. 10, no. 11, pp. 4381–4386, Nov. 2010, doi: https://doi.org/10.1021/nl101902k.

[49] X. Qi, F. Jiang, M. Zhou, W. Zhang, and X. Jiang, “Graphene oxide as a promising material in dentistry and tissue regeneration: A review,” *Smart Mater. Med.*, vol. 2, pp. 280–291, Jan. 2021, doi: 10.1016/J.SMAIM.2021.08.001.

[50] S. Raza, R. Augustine, A. A. Zahid, R. Ahmed, and A. Hasan, “Graphene Oxide Loaded Hydrogel for Enhanced Wound Healing in Diabetic Patients,” in *2019 41st Annual International Conference of the IEEE Engineering in Medicine and Biology Society (EMBC)*, 2019, pp. 3943–3946.

[51] J. He *et al.*, “Killing dental pathogens using antibacterial graphene oxide,” *ACS Appl. Mater. Interfaces*, vol. 7, no. 9, pp. 5605–5611, 2015, doi: 10.1021/acsami.5b01069.

[52] K. Kawamoto *et al.*, “Characterization and evaluation of graphene oxide scaffold for periodontal wound healing of class II furcation defects in dog,” *Int. J. Nanomedicine*, vol. 13, pp. 2365–2376, 2018, doi: 10.2147/IJN.S163206.

[53] S. Lara-Ochoa, W. Ortega-Lara, and C. E. Guerrero-Beltrán, “Hydroxyapatite Nanoparticles in Drug Delivery: Physicochemistry and Applications,” *Pharmaceutics*, vol. 13, no. 10, p. 1642, Oct. 2021, doi: 10.3390/PHARMACEUTICS13101642.

[54] S. Kargozar *et al.*, “Hydroxyapatite Nanoparticles for Improved Cancer Theranostics,” *J. Funct. Biomater. 2022, Vol. 13, Page 100*, vol. 13, no. 3, p. 100, Jul. 2022, doi: 10.3390/JFB13030100.

[55] M. Okada and T. Furuzono, “Hydroxylapatite nanoparticles: fabrication methods and medical applications,” *Sci. Technol. Adv. Mater.*, vol. 13, no. 6, pp. 64103–64117, Dec. 2012, doi: 10.1088/1468-6996/13/6/064103.

[56] Daniela José dos Santos Teixeira, “Síntese e caracterização de nanopartículas magnéticas para aplicação em biomedicina,” 2018.

[57] C. F. Santos, “Synthesis and funtionalization of Hydroxyapatite nanoparticles,” Universidade de Aveiro, 2012.

[58] Y. Li *et al.*, “Polydopamine-mediated graphene oxide and nanohydroxyapatite-incorporated conductive scaffold with an immunomodulatory ability accelerates periodontal bone regeneration in diabetes,” *Bioact. Mater.*, vol. 18, no. February, pp. 213–227, 2022, doi: 10.1016/j.bioactmat.2022.03.021.

[59] F. Vahdatinia *et al.*, “3D-Printed Soft Membrane for Periodontal Guided Tissue Regeneration,” *Materials (Basel).*, vol. 16, no. 4, 2023, doi: 10.3390/ma16041364.

[60] H. Yu *et al.*, “Effects of 3-dimensional Bioprinting Alginate/Gelatin Hydrogel Scaffold Extract on Proliferation and Differentiation of Human Dental Pulp Stem Cells,” *J. Endod.*, vol. 45, no. 6, pp. 706–715, 2019, doi: 10.1016/j.joen.2019.03.004.

[61] S. Zhu *et al.*, “3D printed gellan gum/graphene oxide scaffold for tumor therapy and bone reconstruction,” *Compos. Sci. Technol.*, vol. 208, no. December 2020, 2021, doi: 10.1016/j.compscitech.2021.108763.

[62] H. Lee, J. M. Yoo, N. K. Ponnusamy, and S. Y. Nam, “3D-printed hydroxyapatite/gelatin bone scaffolds reinforced with graphene oxide: Optimized fabrication and mechanical characterization,” *Ceram. Int.*, vol. 48, no. 7, pp. 10155–10163, 2022, doi: 10.1016/j.ceramint.2021.12.227.

[63] “NanoComposix - TEM Nanoparticle Analysis.” https://nanocomposix.com/products/tem-nanoparticle-analysis?variant=14138181572 (accessed Nov. 10, 2023).

[64] A. C. PARREIRA, “Nanopartículas De Compostos Intermetálicos Para a Eliminação De Poluentes Primários,” 2016.

[65] H. Saka, *Transmission Electron Microscopy*. Elsevier Ltd, 2003.

[66] “ATR-FTIR Spectroscopy Fundamentals of Attenuated Total Reflectance (ATR).” https://www.mt.com/in/en/home/applications/L1_AutoChem_Applications/ftir-spectroscopy/attenuated-total-reflectance-atr.html (accessed Nov. 10, 2023).

[67] R. Swetha Sri, K. Bhavya Sri, and B. Benazir, “Attenuated total Reflectance FTIR,” *J. Innov. Pharm. Sci.*, vol. 3, no. 2, pp. 14–17, 2019.

[68] S. Nasrazadani and S. Hassani, *Chapter 2 - Modern analytical techniques in failure analysis of aerospace, chemical, and oil and gas industries*. Elsevier Ltd., 2016.

[69] Thermofisher, “What is SEM? - Scanning Electron Microscopy explained.” https://www.thermofisher.com/blog/materials/what-is-sem-scanning-electron-microscopy-explained/ (accessed Nov. 10, 2023).

[70] “What is Tensile Testing? - TWI.” https://www.twi-global.com/technical-knowledge/faqs/what-is-tensile-testing (accessed Nov. 14, 2023).

[71] Stable Micro Systems, “Texture Analysis Professionals Blog.” https://textureanalysisprofessionals.blogspot.com/2018/09/tensile-testing-using-texture-analyser.html (accessed Nov. 17, 2023).

[72] N. Saba, M. Jawaid, and M. T. H. Sultan, *An overview of mechanical and physical testing of composite materials*. Elsevier Ltd, 2018.

[73] “Allevi 2 - Allevi.” https://www.allevi3d.com/allevi-2/ (accessed Oct. 18, 2023).

[74] B. Gayathri, N. Muthukumarasamy, D. Velauthapillai, S. B. Santhosh, and V. asokan, “Magnesium incorporated hydroxyapatite nanoparticles: Preparation, characterization, antibacterial and larvicidal activity,” *Arab. J. Chem.*, vol. 11, no. 5, pp. 645–654, 2018, doi: 10.1016/j.arabjc.2016.05.010.

[75] M. Salarian, M. Solati-Hashjin, S. Sara Shafiei, A. Goudarzi, R. Salarian, and A. Nemati, “Surfactant-assisted synthesis and characterization of hydroxyapatite nanorods under hydrothermal conditions,” *Mater. Sci. Pol.*, vol. 27, no. 4, pp. 961–971, 2009.

[76] I. F. Mosa, M. Youssef, M. Kamel, O. F. Mosa, and Y. Helmy, “Synergistic antioxidant capacity of CsNPs and CurNPs against cytotoxicity, genotoxicity and pro-inflammatory mediators induced by hydroxyapatite nanoparticles in male rats,” *R. Soc. Chem.*, vol. 8, no. 6, p. 939, 2019, doi: 10.1039/c9tx00221a.

[77] L. Grigorjeva, D. Millers, K. Smits, D. Jankovica, and L. Pukina, “Characterization of hydroxyapatite by time-resolved luminescence and FTIR spectroscopy,” *IOP Conf. Ser. Mater. Sci. Eng.*, vol. 49, no. 1, 2013, doi: 10.1088/1757-899X/49/1/012005.

[78] P. Feng *et al.*, “Hydrothermal synthesis of hydroxyapatite nanorods and their use in PCL bone scaffold,” *Ceram. Int.*, vol. 48, pp. 33682–33692, 2022, doi: 10.1016/j.ceramint.2022.07.314.

[79] J. M. Townsend, E. C. Beck, S. H. Gehrke, C. J. Berkland, and M. S. Detamore, “Flow behavior prior to crosslinking: The need for precursor rheology for placement of hydrogels in medical applications and for 3D bioprinting,” *Prog. Polym. Sci.*, vol. 91, pp. 126–140, Apr. 2019, doi: 10.1016/j.progpolymsci.2019.01.003.

[80] H. Li, S. Liu, and L. Li, “Rheological study on 3D printability of alginate hydrogel and effect of graphene oxide,” *Int. J. Bioprinting*, vol. 2, no. 2, pp. 54–66, 2016, doi: 10.18063/IJB.2016.02.007.

[81] G. Germini and L. Peltonen, “3D Printing of Drug Nanocrystals for Film Formulations,” *Molecules*, vol. 26, no. 13, pp. 1–12, 2021, doi: 10.3390/molecules26133941.

[82] A. M. Wätjen, P. Gingter, M. Kramer, and R. Telle, “Novel prospects and possibilities in additive manufacturing of ceramics by means of direct inkjet printing,” *Adv. Mech. Eng.*, vol. 2014, pp. 1–12, 2014, doi: 10.1155/2014/141346.

[83] S. S. Hossain, H. J. Son, S. Park, and C. J. Bae, “Extrusion-based 3D printing alumina-silica inks: Adjusting rheology and sinterability incorporating waste derived nanoparticles,” *J. Eur. Ceram. Soc.*, vol. 43, no. 11, pp. 4865–4876, 2023, doi: 10.1016/j.jeurceramsoc.2023.03.068.

[84] J. Skopinska-Wisniewska, M. Tuszynska, and E. Olewnik-Kruszkowska, “Comparative Study of Gelatin Hydrogels Modified by Various Cross-Linking Agents,” *Materials (Basel).*, vol. 14, no. 396, pp. 1–15, 2021, doi: 10.3390/ma14020396.

[85] A. Moura, “Engineering a 3D composite hydrogel with antibacterial activity for skin regeneration,” Instituto Superior Técnico, 2021.

[86] I. M. Jipa *et al.*, “Potassium sorbate release from poly(vinyl alcohol)-bacterial cellulose films,” *Chem. Pap.*, vol. 66, no. 2, pp. 138–143, 2012, doi: 10.2478/s11696-011-0068-4.

[87] P. Sun and Q. Li, “Tension-Responsive Graphene Oxide Conductive Hydrogel with Robust Mechanical Properties and High Sensitivity for Human Motion Monitoring,” *Macromol. Mater. Eng.*, vol. 308, no. 4, pp. 1–10, 2023, doi: 10.1002/mame.202200529.

[88] N. Rashid *et al.*, “Curcumin-Loaded Bioactive Polymer Composite Film of PVA/Gelatin/Tannic Acid Downregulates the Pro-inflammatory Cytokines to Expedite Healing of Full-Thickness Wounds,” *ACS Omega*, vol. 8, no. 8, pp. 7575–7586, 2023, doi: 10.1021/acsomega.2c07018.

[89] Merck, “IR Spectrum Table & Chart.” https://www.sigmaaldrich.com/PT/en/technical-documents/technical-article/analytical-chemistry/photometry-and-reflectometry/ir-spectrum-table (accessed Nov. 07, 2023).

[90] R. C. Simoni *et al.*, “Effect of drying method on mechanical, thermal and water absorption properties of enzymatically crosslinked gelatin hydrogels,” *An Acad Bras Cienc*, no. 1, pp. 745–755, 2017, doi: 10.1590/0001-3765201720160241.

[91] A. K. Gaharwar, S. A. Dammu, J. M. Canter, C. J. Wu, and G. Schmidt, “Highly extensible, tough, and elastomeric nanocomposite hydrogels from poly(ethylene glycol) and hydroxyapatite nanoparticles,” *Biomacromolecules*, vol. 12, no. 5, pp. 1641–1650, 2011, doi: 10.1021/bm200027z.

[92] B. Lian *et al.*, “Extraordinary water adsorption characteristics of graphene oxide,” *Chem. Sci.*, vol. 9, no. 22, pp. 5106–5111, 2018, doi: 10.1039/c8sc00545a.

[93] C. Chen, H. Yang, X. Yang, and Q. Ma, “Tannic acid: a crosslinker leading to versatile functional polymeric networks: a review,” *RSC Adv.*, vol. 12, no. 13, pp. 7689–7711, Mar. 2022, doi: 10.1039/D1RA07657D.

[94] R. Parhi, “Cross-Linked Hydrogel for Pharmaceutical Applications: A Review,” *Tabriz Univ. Med. Sci.*, vol. 7, no. 4, pp. 515–530, 2017, doi: 10.15171/apb.2017.064.

[95] A. Jiříčková, O. Jankovský, Z. Sofer, and D. Sedmidubský, “Synthesis and Applications of Graphene Oxide,” *Materials (Basel).*, vol. 15, no. 3, 2022, doi: 10.3390/ma15030920.

[96] A. Vaidya and K. Pathak, *Mechanical stability of dental materials*. Elsevier Inc., 2019.

[97] K. H. Kang, L. A. Hockaday, and J. T. Butcher, “Quantitative optimization of solid freeform deposition of aqueous hydrogels,” *Biofabrication*, vol. 5, no. 3, Sep. 2013, doi: 10.1088/1758-5082/5/3/035001.

[98] T.-S. Jang, H.-D. Jung, H. M. Pan, W. T. Han, S. Chen, and J. Song, “3D Printing of hydrogel composite systems: Recent advances intechnology for tissue engineering,” 2018, doi: 10.18063/IJB.v4i1.126.

[99] S. Wüst, M. E. Godla, R. Müller, and S. Hofmann, “Tunable hydrogel composite with two-step processing in combination with innovative hardware upgrade for cell-based three-dimensional bioprinting,” *Acta Biomater.*, vol. 10, no. 2, pp. 630–640, Feb. 2014, doi: 10.1016/J.ACTBIO.2013.10.016.

[100] J. Li *et al.*, “Development of 3D printable graphene oxide based bio-ink for cell support and tissue engineering,” 2022, doi: 10.3389/fbioe.2022.994776.

[101] S. B. Qasim, R. M. Delaine-Smith, T. Fey, A. Rawlinson, and I. U. Rehman, “Freeze gelated porous membranes for periodontal tissue regeneration,” *Acta*, vol. 23, pp. 317–328, 2015, doi: 10.1016/j.actbio.2015.05.001.

[102] P. Y. Wong *et al.*, “A Novel Antimicrobial Hydrogel for the Management of Periodontal Diseases,” *Int. Dent. J.*, vol. 73, no. 3, pp. 354–361, Jun. 2023, doi: 10.1016/J.IDENTJ.2023.01.002.